ORIGINAL RESEARCH ARTICLE

The Depositional Record
A journal of the International Association of Sedimentologists
Open Access
IAS WILEY

Mechanisms controlling the localisation of fault-controlled hydrothermal dolomitisation, Derbyshire Platform, UK

Catherine J. Breislin[1] | Vanessa J. Banks[2] | Stephen F. Crowley[3] | Jim D. Marshall[3] | Ian Millar[2] | James B. Riding[2] | Cathy E. Hollis[1]

[1]School of Earth, Atmospheric and Environmental Sciences, University of Manchester, Manchester, UK

[2]British Geological Survey, Nottingham, UK

[3]Department of Earth, Ocean and Ecological Science, University of Liverpool, Jane Herdman Laboratories, Liverpool, UK

Correspondence
Cathy E. Hollis, School of Earth, Atmospheric and Environmental Sciences, University of Manchester, Williamson Building, Manchester M13 9PL, UK.
Email: cathy.hollis@manchester.ac.uk

Funding information
Natural Environment Research Council, Grant/Award Number: NE/L002469/1

Abstract

The Derbyshire Platform is a Mississippian aged flat-topped, steep sided platform that forms the westernmost expression of the Derbyshire-East Midlands Platform. On the south-east platform margin, $60\,km^2$ of Visean limestone has been dolomitised, forming two distinct bodies. One of these bodies forms along a major NW–SE trending basement fault and smaller, associated, N–S trending faults and fractures. This study uses outcrop, petrographic and geochemical analysis to better constrain the timing and mechanism for this fault-controlled dolomitisation. Field relationships demonstrate dolomitisation was multi-phase and initiated after the main phase of matrix pore-occluding calcite cementation on the Derbyshire Platform and terminated prior to the main phase of mineralisation. Fluids are interpreted to have fluxed from adjacent basins, primarily along strike-slip crustal faults that were reactivated during basin inversion at the onset of the Variscan Orogeny. Fluid supply was episodic and progressively confined to fractures as matrix porosity became occluded. The study demonstrates the complex interplay between basin kinematics, host rock permeability and timing of fluid supply through seismic valving along faults that connect the carbonate platform to basin compartments. This ultimately controlled the position of dolomite geobodies along faults and provides a record of fluid flow during the transition from thermal subsidence to post-rift basin inversion. The findings have implications for the exploration of both minerals and hydrocarbon within dolomitised host rocks and can inform studies of fluid transfer and reaction on carbonate platforms within the burial realm.

KEYWORDS
dolomite, fault, structural diagenesis, Visean

---

1 | INTRODUCTION

The processes governing dolomitisation from hot, sometimes hydrothermal, fluids has received much interest as the resultant dolomite bodies are often important hosts for Mississippi Valley type (MVT) mineralisation and hydrocarbons (Davies & Smith, 2006; Ehrenberg et al., 2006; Ford, 2001; Ford & Quirk, 1995; Ibrahem et al., 2021; Korneva et al., 2018; Omidpour et al., 2022; Saller & Dickson, 2011). Dolomite bodies can also be an excellent proxy for fluid flow and reaction in carbonate systems (Hollis et al., 2017; Koeshidayatullah et al., 2020). However, the source, mass balance and chemistry of the fluids necessary to form these often large volumes of dolomitised limestone are not always easy to constrain (Davies & Smith, 2006; Machel & Lonnee, 2002; Saller & Dickson, 2011; Whitaker et al., 2004). The integration of hydrological and reactive transport models can be extremely powerful in reconstructing palaeo-fluid flow and reaction (Benjakul et al., 2020; Corbella et al., 2014; Frazer et al., 2014), supported by a comprehensive understanding of basin-scale tectonics and platform evolution (Hollis et al., 2017; Stacey et al., 2020, 2021). This paper addresses this issue within the Derbyshire Platform in the Pennine Basin in northern England, which has a well-constrained tectono-stratigraphy and has previously been modelled using reactive transport and fluid flow models.

In the Pennine Basin and North Wales, UK (Figure 1), fault-controlled dolomite bodies are developed on the margins of Mississippian carbonate platforms that grew on the rotated footwalls of normal faults and a basement of Lower Palaeozoic metasediments (Bouch et al., 2004; Ford, 2002; Fowles, 1987; Frazer, 2014; Frazer et al., 2014; Gawthorpe, 1987; Hollis & Walkden, 2002, 2012; Juerges et al., 2016; Schofield & Adams, 1986). Dolomite is also observed within basinal sediments (Bouch et al., 2004; Breislin, 2018; Frazer et al., 2014; Gawthorpe, 1987). Although these dolomite bodies have been studied previously, there has been little recent, detailed analysis of the largest body (>50 km^2) on the Derbyshire Platform (Bouch et al., 2004; Breislin, 2018; Ford, 2002; Fowles, 1987; Schofield & Adams, 1986). This dolomite body is significantly larger than the North Wales Platform (ca 8 km^2; Juerges et al., 2016) and the Askrigg Platform (ca 20 km^2; Hollis & Walkden, 2012). There is also a lack of consensus as to the mechanism by which it formed. Fowles (1987) proposed dolomitisation by downward-seeping brines in the Permo-Triassic while Ford (2002), Hollis and Walkden (2012) and Frazer et al. (2014), proposed dolomitisation, at least in part, from basinal brines expelled from Visean sediments within juxtaposed hangingwall basins.

FIGURE 1 Tectonic setting for the Mississippian of England, Wales and southern Scotland, after Fraser and Gawthorpe (2003); BH—Bowland high; BT—Bowland Trough; CLH—Central Lancashire high; DF—Dent Fault; DP—Derbyshire Platform; FHF—Flamborough Head Fault; GT—Gainsborough Trough; HdB—Huddersfield Basin; HB—Humber Basin; LDH—Lake District high; MCF—Morley-Campsall Fault; MH—Manx high; NCF—North Craven Fault; PF—Pennine Fault; SF—Stublick Fault; WG—Widmerpool gulf. The yellow box highlights the position of the Derbyshire Platform, the focus of this study.
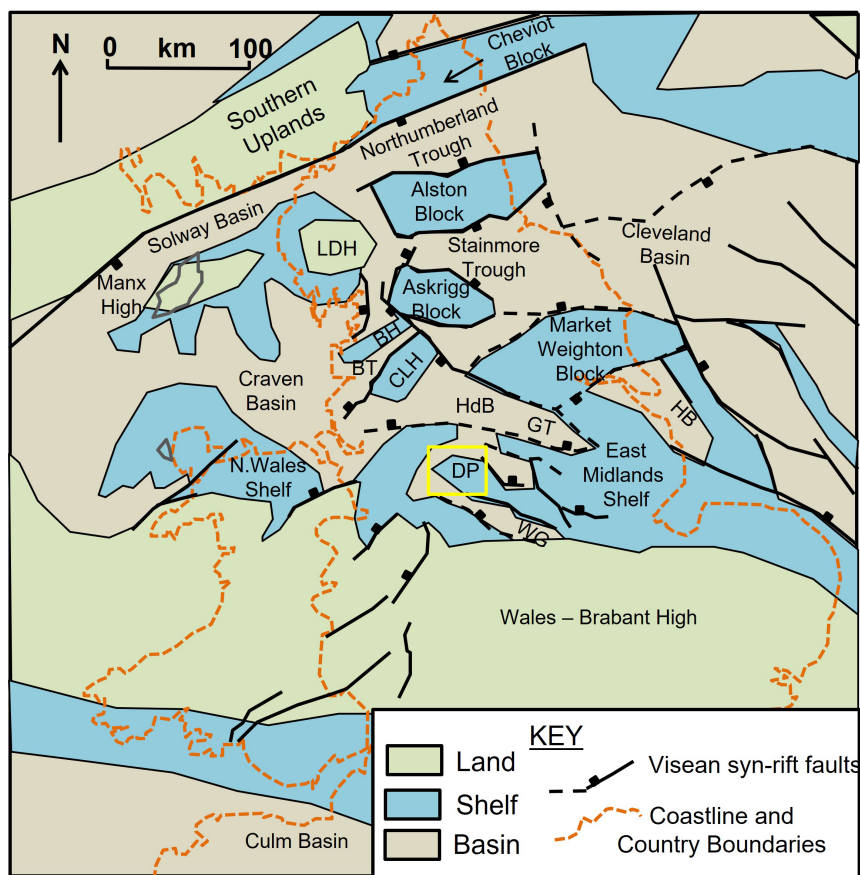
Similar models have been presented for other platforms (Bouch et al., 2004; Gawthorpe, 1987; Juerges et al., 2016). On all platforms, dolomitisation appears to be associated with major basement fault zones.

Frazer et al. (2014) showed that dolomitisation could have been initiated on the southern margin of the Derbyshire Platform by syn-depositional convection of sea-water, facilitated by high heat flows during intraplate volcanic activity (Macdonald et al., 1986). Breislin et al. (2020) mapped this dolomite body and showed that it was not entirely fault-controlled and presented petrographical and geochemical evidence for dolomitisation from sea-water. This first phase of dolomite is referred to as 'D1' and is cross-cut by four later phases of fault-controlled dolomite on the Derbyshire Platform (D2–D5). This paper examines the geometry of these D2–D5 dolomite bodies, the controls on their distribution, and the tectonostratigraphic controls on their formation.

2 | GEOLOGICAL SETTING

This paper focusses on the characterisation of a pervasively dolomitised area of Visean (Asbian and Brigantian) limestone on the southern margin of the Derbyshire Platform (Figure 2). Across the Pennine Basin, back-arc extension during the Visean formed E–W trending normal faults and reactivated pre-existing, NE–SW and NW–SE trending, Caledonian faults. During the Tournasian, carbonate sediments were deposited on a gently sloping carbonate ramp (Woo Dale Limestone Formation; Schofield & Adams, 1986; Bridges & Chapman, 1988). By the Visean, there was a clear differentiation between flat-topped, steep sided, carbonate platforms on footwalls and deposition of finer grained sediment in deeper water within hangingwall basins (Fraser & Gawthorpe, 2003). Platform top facies are characterised by a thick succession of skeletal wacke-packstones and grainstones with frequent emergent surfaces within the Asbian succession (Bee Low Limestone Formation), overlain by finer grained, chert-rich Brigantian wacke-packstones (Monsal Dale Limestone and Eyam Limestone formations) (Manifold et al., 2020). The boundary between the Asbian and Brigantian is marked by a karstic surface, identifiable across the platform (Manifold et al., 2021). Emergent surfaces are evidenced by the presence of mamillated surfaces (Vanstone, 1998), palaeosols rich in volcanic ash and lava flows proximal to the igneous centres (Walkden, 1972). In the basins, the Asbian–Brigantian succession comprises carbonate turbidites, which grade upwards from limestone-dominated (e.g. Ecton Limestone Formation) into deeper water mudstones with limestone and sandstone turbidites (e.g. Widmerpool Formation). Extension waned

during the Serpukhovian, leading to post-rift thermal sag subsidence (Collinson, 1988; Guion & Fielding, 1988; Leeder, 1988), prior to the Variscan Orogeny which resulted in basin inversion along reactivated NW–SE trending strike-slip faults (Fraser & Gawthorpe, 2003).

3 | DOLOMITISATION

Dolomite on the Derbyshire Platform occurs principally in two localities, within Asbian and Brigantian (upper Visean) limestone, forming non-stratabound sub-bodies bounded by NW–SE orientated crustal faults (Figure 2). In nearly all cases, dolomite bodies have a diffuse, irregular lower contact, which is rarely seen, approximately 40 m (but locally up to 120 m) beneath the top Brigantian (Breislin et al., 2020; Ford, 2002). Dolomitisation pre-dates calcite-baryte-galena-fluorite mineralisation (Breislin et al., 2020; Frazer, 2014) and forms five discrete phases (Table 1; Breislin, 2018; Breislin et al., 2020). D1 dolomite occurs primarily on the platform margin and forms halos along E–W orientated faults, particularly in proximity to the Masson Hill volcanic centre (Breislin et al., 2020). In outcrop, it is fabric retentive, largely stratabound, buff-grey in colour and sucrosic in texture. Petrographically, D1 is characterised by limpid, planar dolomite with a yellow-orange luminescence (Breislin et al., 2020). This study focusses on the subsequent phases of dolomitisation, D2–D5 which are described in detail later and in Table 1.

A third dolomite body forms on the Derbyshire Platform in the lower part of the Woo Dale Limestone Formation (so-called Woo Dale Dolomite, Tournasian - Visean). It is laterally restricted (<5 km^2), outcropping exclusively within the Wye Valley inlier as laterally continuous beds and irregular cross-cutting dolomite bodies (Schofield & Adams, 1986), and was not included in this study.

4 | DIAGENETIC FRAMEWORK

The diagenetic history of the Visean succession of the Derbyshire Platform is well-constrained (Gutteridge, 1987, 1991; Hollis, 1998; Hollis & Walkden, 2002; Walkden & Williams, 1991). Four major phases of calcite cementation (Zones 1–4) were described by Walkden and Williams (1991). Zones 1 and 2 were interpreted to form in the meteoric phreatic realm, while Zone 3 calcite precipitated in the shallow burial realm from fluids which were driven down depositional dip by topographic flow (Walkden & Williams, 1991). Zone 3 is the major pore-occluding phase and is succeeded by minor volumes of Zone 4 calcite, which occluded matrix porosity and fractures (Hollis, 1998; Hollis & Walkden, 1996, 2002). These
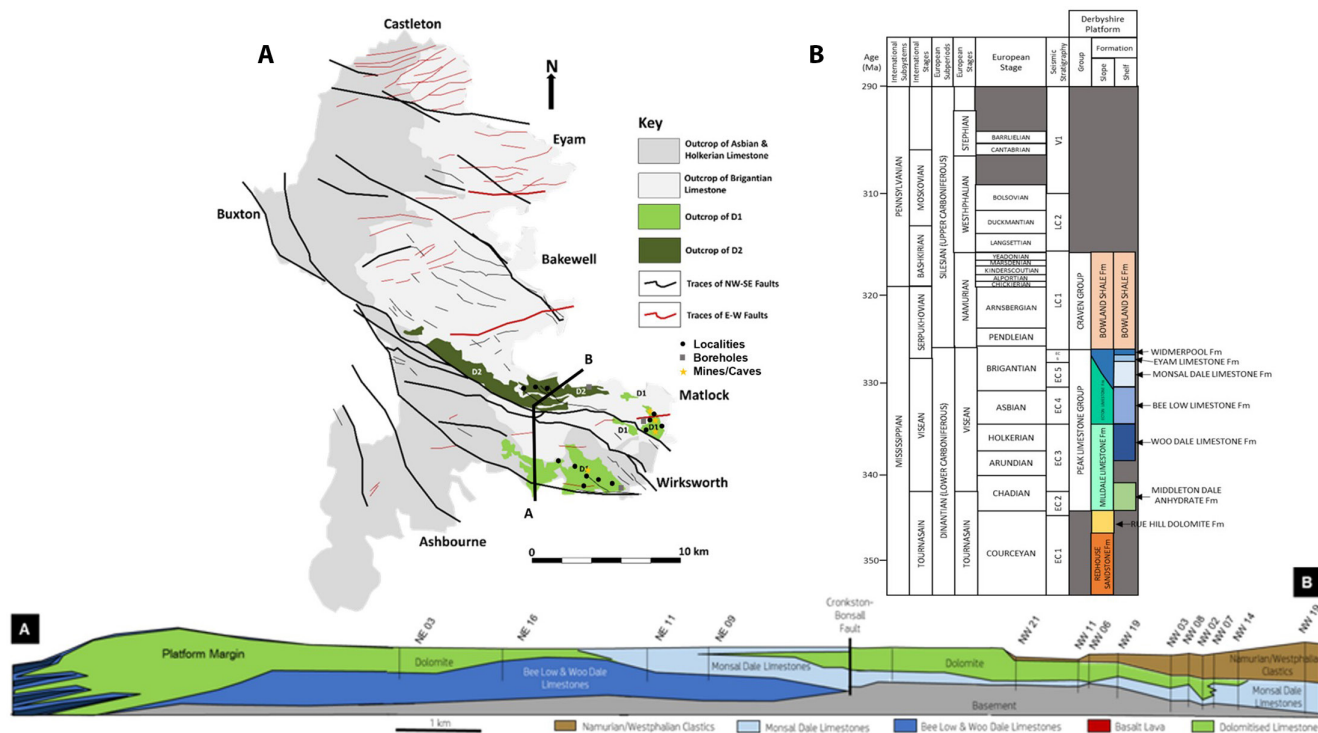
FIGURE 2 (A) Geological map of the Derbyshire Platform. Sample localities, boreholes and mine/caves are identified on the map; black circles represent localities; (B) Lithostratigraphy after Fraser and Gawthorpe (2003) with Visean lithology (EC2-EC6); (C) cross-section A–B (shown on A) of the southern margin of the Derbyshire Platform, showing facies distribution and distribution of D1 dolomite (green). Vertical exaggeration on cross-section ×4.

Zone 4 cements are interpreted to have co-precipitated with fluorite, sulphates and sulphides that have been mined within the region, and hydrocarbon (Hollis & Walkden, 2002).

Zone 3 and 4 cements were further subdivided, where they occur within NE–SW and NW–SE fractures and faults, into six sub-zones (Hollis, 1998; Hollis & Walkden, 1996, 2002; Table 2). Fluorite and baryte are intergrown with Zones 3B–4B, which contain abundant hydrocarbon inclusions and are also associated with liquid hydrocarbon and solid bitumen deposits (Hollis & Walkden, 1996, 2002). From Zone 4C onwards, intergrowths of galena and sphalerite also occur. Fluid inclusion homogenisation temperatures can be seen to generally increase from Zones 3A to 4A, reaching a maximum in Zones 4B-C, along with a broad increase in salinity, although fluid salinities are wide-ranging in Zones 4B-C (Hollis & Walkden, 1996, 2002). Burial calcite cements (Zones 3A-B and Zones 4A-D) were interpreted by Hollis (1998) and Hollis and Walkden (1996, 2002) to be co-eval with mineralisation, forming from fluids released from Visean and Serphukhovian sediments within the adjacent Edale, Widmerpool and Staffordshire basins. Frazer et al. (2014) showed that these fluids could have been expelled along faults as a result of rupture of overpressured basinal sediments during the Variscan Orogeny.

5 | METHODS

Thirty-four outcrops and 13 boreholes within the Asbian to Brigantian succession of the Derbyshire Platform were described by sedimentological logging (of texture, compositional changes, sedimentary features, skeletal content and diagenetic features). Cross-sections (Figure 2) were constructed using borehole data from the British Geological Survey and the Groundhog software suite in order to define the known distribution of the dolomite body.

Each locality was sampled systematically to cover the stratigraphy and range of lithofacies. A total of 118, 40 μm thick, blue-dye resin-impregnated polished thin sections were prepared. All thin sections were examined using optical transmitted light and cathodoluminescence (CL) microscopy to differentiate replacive dolomite and carbonate cement textures and luminescence characteristics. All thin sections were scanned using an EPSON Perfection V600 Photo at 2,400 dpi resolution. Optical microscopy was undertaken using a Nikon Eclipse LV100NPOL microscope fitted with a Nikon DS-Fi2 camera. Cathodoluminescence observations were made using a CITL CCL 8200 Mk3 'cold' cathode device coupled with a Progress C10 Laser Optik digital photographic system. Operating conditions for

TABLE 1 Summary of the five dolomite phases identified on the Derbyshire Platform and their structural relationships, from Breislin et al. (2020).

Phase	Field distribution	Morphology	Structural trend	Colour (hand specimen)	Texture (microscopic)	CL	Inclusions	Volume (%)
D1	Stratabound	Replacive, fabric retentive and sucrosic (in outcrop)	E–W	Buff-grey	Planar	Yellow-Orange	Limpid, minor single phase aqueous inclusions	50
D2	Non-stratabound	Replacive, non-fabric retentive (in outcrop)	NW–SE	Grey	Non-planar, dark brown, 0.2–0.8 mm	Bright red-orange	Inclusion-rich (2 phase aqueous and hydrocarbon)	40
D3			N–S	Grey	Non-planar, dark brown, 0.1–0.6 mm	Dull red		<10
D4		Cement	NW–SE; N–S; NE–SW	Red-pink	Non-planar and saddle, <0.4 mm	Dull red	Inclusion-rich (2 phase aqueous)	<5
D5				White	Saddle, 0.3–0.8 mm	Bright red		<5

TABLE 2 Calcite cement phases described by Hollis and Walkden (1996, 2002) and their geochemistry, with the range of possible $\delta^{18}O_{water}$ values for each phase calculated using average $\delta^{18}O_{carbonate}$ and average homogenisation temperature, using the fractionation equation of Wostbrock et al. (2020).

Calcite cement	Cathodo-luminescence	$\delta^{13}C$ (‰ PDB)	$\delta^{18}O$ (‰ PDB)	Homogenisation temperature (°C)	Fluid salinity (wt% NaCl equiv)	$\delta^{18}O_{water}$ (‰ SMOW)	Mineral associations	Hydrocarbon
Zone 1	Non-luminescent	−3.4 to −1.7	−9.6 to −6.8	—	—	—	—	—
Zone 2	Bright	—	—	—	—	—	—	—
Zone 3A	Dull brown	2.3 (0.7 to 3.7)	−10.3 (−12.3 to −7.6)	57.3 (35.6–80.6)	5.8 (0.75–13)	−2.8	—	—
Zone 3B	Dull brown	1.1 (−3.3 to 4.1)	−8.9 (−14.0 to −4.8)	106 (82.2–125)	4.4 (0.17–18.1)	4.9	Silica, fluorite, pyrite	Present
Zone 4A	Dull orange	0.4 (−2.0 to 3.3)	−6.1 (−5.8 to −2.7)	136 (124–153)	16.4 (14.3–17.4)	10.6	Silica, pyrite, fluorite	Present
Zone 4B	Dull brown – orange (concentric zonation)	2.0 (0.3–3.3)	−8.5 (−9.9 to −5.8)	176 (148–200)	7.7 (0.16–22.2)	11.0	Silica, pyrite, sphalerite, baryte, fluorite	Present
Zone 4C	Bright orange	2.3 (0.7–to 2.9)	−7.5 (−9.5 to −6.2)	168 (117–207)	9.4 (0.66–23.1)	11.5	Baryte, fluorite, sphalerite, galena	Present
Zone 4D	Bright orange	1.1 (−0.7 to 2.8)	−7.5 (−7.8 to −6.5)	—	—	—	—	—

CL were set to 10 kV and 300 μA at a pressure of *ca* 0.2 torr and maintained by microcomputer control. For one sample, Quantitative Evaluation of Minerals by Scanning Electron microscopy (QEMSCAN) was undertaken in the Williamson Research Centre, University of Manchester, comprising a Bruker XFlash energy dispersive X-ray spectrometer (EDS) and backscattered secondary electron (BSE) image. The brightness of the BSE is calibrated to quartz standards and the EDS spectra acquired using thousand counts/pixel, measured at the centre of each pixel. A mineralogy map for one sample was constructed using QEMSCAN IExplore software® and was used to refine paragenetic relationships defined using transmitted light and CL petrography.

X-ray diffraction (XRD) was conducted on powdered samples to confirm the mineralogy of the rock and determine dolomite stoichiometry and ordering. Samples were acquired using a precision drill, prepared following the methodology of Charlier et al. (2006) and analysed using a Bruker D8 Advance diffractometer at the University of Manchester using Cu k α_{1+2} radiation, a tube voltage of 40 kV and a tube current of 40 mA. Samples were scanned between X °2θ and XX °2θ using a step size of 0.02 °2θ and time interval of 2.00 s per step. Semi-quantitative estimates of bulk mineralogy fractions were carried out using peak area measurements (sensu Schultz, 1964). All results contain an analytical error of 0.05.

To measure the concentration of trace elements within individual carbonate phases, inductively coupled plasma mass spectrometry (ICP-MS) analysis was conducted on powdered samples (100 mg per sample) of host rock limestone, bulk replacive dolomite and individual cement zones. Corresponding samples were drilled from hand specimens and their purity checked by XRD. Samples were digested in 2 ml of 20% HCl and left to react for 24 h before dilution with deionised water to 2% HCl and left to react for a further 24 h. Samples were microwaved for 60 min at 50°C, before adding 10 ml of de-ionised water and centrifuging at 3,000 rpm for 10 min. Finally, 5 ml of supernatant from each sample were removed before placing in a new centrifuge tube and diluted by adding 10 ml of de-ionised water, ensuring that the total dissolved solids of each sample was less than 0.1%. Two blank samples were prepared in the same way for reproducibility and samples were run against internal standards with a detection limit of 0.01 ppb and reproducibility of 0.1‰ (1σ). Rare earth elements (REE) and Y concentrations were then measured using an Agilent 7500cx mass spectrometer Advanced Isotope Geochemistry and Cosmochemistry Suite at the University of Manchester. All samples are reported in mg/L or μg/L (ppm or ppb) and were then normalised to Post-Archean Australian Shales (PAAS) following the methods of Nance and Taylor (1976).

Stable isotope analysis was conducted on powdered samples of dolomite, limestone, brachiopods and discrete cement phases of dolomite and calcite to assess the origin of dolomitising fluids. Samples were acquired using a tungsten-tipped, 0.05 mm drill bit mounted on a hand-held dentist drill. The rock sample was cleaned between collection of each powder sample using pressurised air and deionised water and the drill bit cleaned using 0.5% HCl. The mineralogy of samples was determined by XRD prior to analysis; partially dolomitised samples were not analysed. Stable isotope analysis of powdered (4.5 mg) samples was conducted at the University of Liverpool. Carbon dioxide for mass spectrometric analysis (sensu McCrea, 1950) was prepared from samples of calcite and dolomite by reaction with phosphoric acid (specific gravity 1.92) at temperatures of 25°C (for 16 h) and 60°C (for 24 h) respectively. Gases were measured by dual-inlet, stable isotope ratio mass spectrometry using a VG SIRA 10 mass spectrometer. Isotope ratios were corrected for ^{17}O effects following the methods of Gonfiantini (1981) and calibrated to the Vienna Pee Dee belemnite (VPDB) international reference framework using a single-point procedure based on the contiguous multi-replicate measurement of an in-house Carrara marble (calibrated against NBS18 and NBS19). Oxygen isotope data were adjusted for isotopic fractionation associated with the calcite-phosphoric and dolomite-phosphoric acid reactions using fractionation factors (σ) of 1.01025 (Friedman & O'Neil, 1977) and 1.01028 (Rosenbaum & Sheppard, 1986). All results are reproducible to $< \pm 0.1‰$.

To further constrain the origin of dolomitising fluids, strontium isotopic analysis was conducted at the Geochronology and Tracers Facility, British Geological Survey. Powdered whole rock and discrete dolomite cements were obtained using a tungsten-tipped micro-mill following the methodology of Charlier et al. (2006) and Pollington and Baxter (2010). Sample purity was checked where necessary by XRD. Samples were spiked with ^{84}Sr in order to allow calculation of strontium concentrations, prior to dissolution using A-grade acetic acid. Strontium was extracted from the rock powders for isotopic analysis using Sr-Spec chromatographic resin. Column preparation and chemical separation were conducted following the methodology of Deniel and Pin (2001) and Charlier et al. (2006). Samples were loaded on to single rhenium filaments using a TaO emitter solution and analysed on a Thermo Scientific Triton thermal ionisation mass spectrometer. Samples were run in two analytical sessions. Across the time of the first session, 39 analyses of the NBS987 reference material gave an $^{87}Sr/^{86}Sr$ value of 0.710253 ± 0.000006 (8.4 ppm, 1-sigma). Across the time of the second session, 18 analyses of NBS987 gave a value

of 0.710262 ± 0.000005 (7.2 ppm, 1-sigma). Results are reported relative to a value of 0.710250 for the reference material.

Fluid inclusion microthermometry was carried out on selected dolomite and calcite specimens using a Linkham TH600 heating-freezing stage, controlled by Linksys32 software and a Linkam TP93 programmer. The homogenisation temperature (Th) provides an estimate of the temperature of mineral precipitation, while the last ice melting temperature (T_m) provides information on fluid salinity. Samples were prepared as 150 μm double-polished wafers. Care was taken to analyse primary or pseudo-secondary inclusions based on careful petrography, including distribution within crystals and consistent size and liquid: vapour ratios (Goldstein & Reynolds, 1994). Homogenisation temperatures (Th) and last ice melting temperatures (T_m) are reproducible to ±2°C and ±0.2°C, respectively. No pressure corrections were made to Th data, because it was not possible to unambiguously determine burial depth at the time(s) of precipitation.

6 | RESULTS

6.1 | Distribution of dolomite

Whereas D1 dolomite occurs primarily on the southern margin of the Derbyshire Platform (Figure 2), phases D2–D5 dolomite are largely found along faults and fractures that dissect the platform. They occur principally within an area that is approximately 2 km north of the southern platform margin, in the vicinity of the NW–SE trending Cronkston–Bonsall Fault, which extends in a north-westerly direction towards the western platform margin (Figure 2). This large fault is approximately 20 km in length, slightly sinuous and sometimes compound, with multiple parallel fractures forming a damage zone around the fault which ranges in thickness from 200 m wide in the north-west to over 3 km wide in the south-east. To the east, the dolomite body extends away from the Cronkston–Bonsall Fault along a fault splay, whereas in the north-west, it becomes more confined, forming a halo up to 200 m thick within the fault damage zone (Figure 2). Along faults, the dolomite is usually pervasive, finely crystalline and fabric destructive, with a dark brown to buff colour (Figure 3). At the western termination of the body, dolomite forms halos along NW–SE and NE–SW trending fault splays, that extend approximately 100 m away from the main fault, within the Asbian Bee Low Limestone Formation. The extent of dolomitisation becomes heterogeneous along the fault plane (Figure 4), where it has also been dedolomitised (not shown). Four fault and fracture controlled dolomite phases are identified, (D2–D5) with D2 having the greatest volume (*ca* 60%). Each successive phase of dolomite becomes increasingly confined to the fault and fracture planes. Phases D2 and D3 are replacive, while phases D4 and D5 are fracture lining and fracture filling
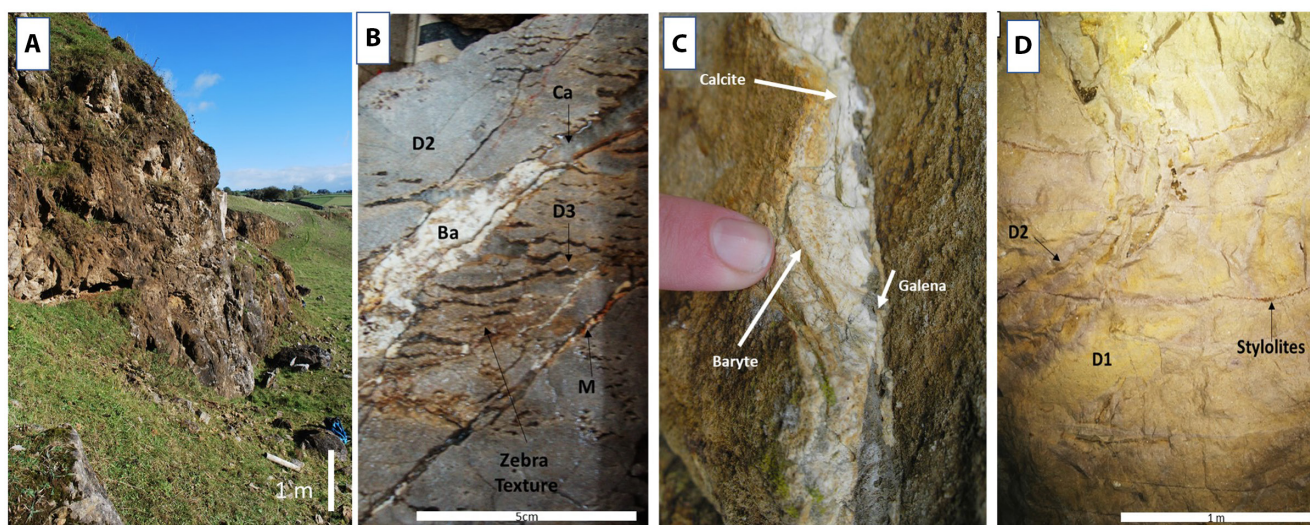

FIGURE 3   D2 dolomite in core and outcrop; (A) D2 dolomite along Eldon Rake Fault; (B) zebra fabric within dolomite D2, observed within four lanes Wirksworth borehole. Zebra fabric forms off fracture. Limestone is fully dolomitised by D2. Zebra fabric also shows dolomitisation by D3, with brown halos formed to fractures. Fracture contains later calcite cement (Ca) and baryte (Ba) mineralisation. Zebra fabric is seen to be cross-cut by later fractures that host calcite, fluorite and baryte mineralisation (arrowed, M); (C) Zone 4 calcite cemented fracture, intergrown with baryte and galena cutting D2 dolomite. (D) Dolomite phase D2 forming along fractures within earlier formed D1 in Golconda mine at the platform margin. Recrystallisation of D1 occurs around these fractures, forming a non-planar mosaic, with low visible porosity. These fractures are seen to cross-cut horizontal stylolites.

FIGURE 4 Dolomite front at the western termination of the northern dolomite geobody at Parsley Hay: the dolomite front displays fracture-controlled dolomitisation and a facies control on distribution. Limestone is shown in blue and dolomite that has formed around fractures (black lines) is shown in green. This dolomite is now dedolomitised.

cements. Their characteristics are described in detail below and in detail in Table 1.

6.2 | Dolomite D2

Dolomite phase 2 (D2) is the most volumetrically significant phase of fault-controlled dolomite (40% total dolomite volume; Table 1) and forms principally along the fault plane and within the damage zone of NW–SE orientated faults. It is non-fabric selective, non-stratabound and fabric destructive, occurring within Asbian and Brigantian bedded packstones, wackestones, mudstones and reef mounds within the platform interior (Figures 2 and 3). It is grey, fine-medium crystalline with mouldic porosity. D2 usually has a sharp, non-fabric selective reaction front, although at the northernmost tip of the main body the dolomite is more fabric selective. Here it forms fingers that extend laterally away from NW–SE faults and fractures while un-replaced limestone is clay rich (Figure 4). Very rarely, D2 contains zebra dolomite textures, which are usually seen in core (Figure 3). D2 cross-cuts stylolites and is locally observed replacing phase D1, altering the colour from buff (D1) to grey (D2) (Figure 3).

D2 is fabric destructive in thin section and is composed of turbid, planar, rarely planar-s, non-ferroan rhombs,

distinguishing it clearly from the planar, limpid crystals of D1 dolomite. Most commonly, the dolomite is non-planar, dark brown and inclusion rich, with crystal sizes of <0.5 mm (Figure 5). Fluid inclusions are two-phase, and some hydrocarbon inclusions were observed. Under CL, the dolomite has a mottled bright red-orange colour, with no zoning (Figure 5B,F). Less commonly, cloudy core - clear rimmed dolomite (Figure 5A) occurs. Crystal size is larger than the non-planar dolomite (0.2–0.8 mm) with inclusion rich centres displaying bright red luminescence under CL and rims of clearer, dull red luminescent dolomite.

Isotopic values of dolomite D2 range from $\delta^{13}C = -1.2$ to 2.4‰ and $\delta^{18}O = -3$ to -7.2‰ (n = 14) (Figure 6). The mean $\delta^{13}C$ values ($\delta^{13}C = 0.8$‰, n.14) of the dolomite is similar, to slightly higher than whole rock limestone and unaltered brachiopods ($\delta^{13}C$ values = 1.2‰ and 0.5‰ respectively). The strontium ratio varies from $^{87}Sr/^{86}Sr = 0.7085$ to 0.7094 (±0.00004) (n.7) (Figure 6B), with an average $^{87}Sr/^{86}Sr$ of 0.7087 to (±0.00004). Strontium concentrations of phases D2 and D3 range from 29 to 57 ppm (n.5) with an average of 37 ppm. The REE patterns for D2 resemble whole rock limestone and brachiopod samples with a relatively large negative cerium anomaly, and a flatter heavy rare earth element (HREE) profile than phase D1 (Figure 7A). Compared to the whole rock limestone and brachiopod samples, the dolomite profile
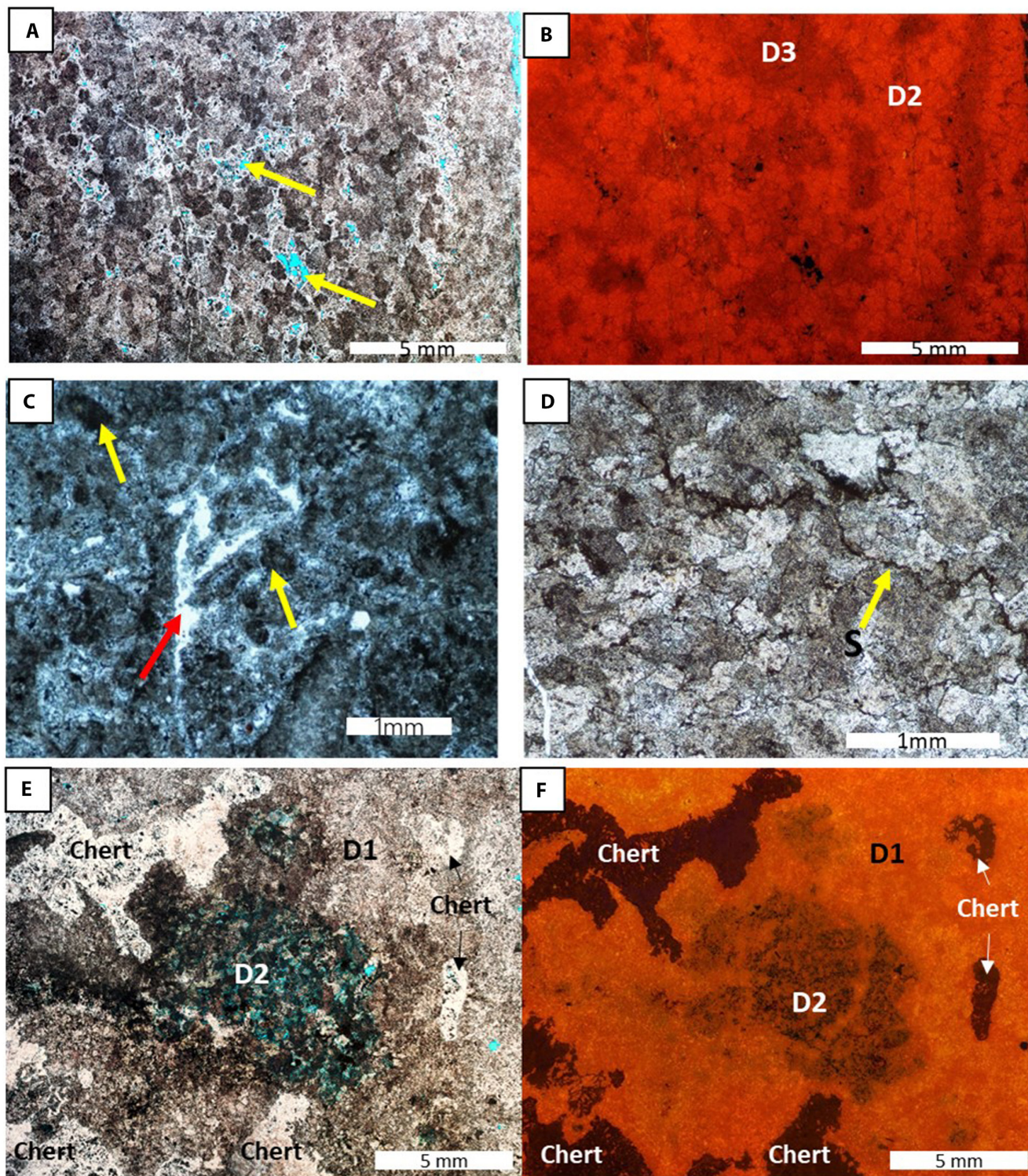
FIGURE 5 D2 petrography; (A) PL, cloudy-core clear-rim texture in planar-s D2. Turbid fluid inclusion density within cores. Intercrystalline porosity developed (arrows); (B) CL, D2 has bright red luminescence, with rims of dolomite crystals having dull red colour. Overprinting of D2 by D3 is patchy, observed by the colour change from bright to dull red and the development of clear rim textures. Where D2 is not overprinted, no cloudy-core clear-rim textures are observed; (C) PL, non-planar, inclusion rich D2, with ghost allochems (yellow arrows) and post-dolomitisation calcite cement occluding porosity (red arrow) (D) PL, planar-s to non-planar D2, seen to cross-cut stylolite (arrow). Dolomite crystals have high inclusion density, and visible porosity is low; (E) PL, D1 showing alteration by D2. D1 presents a planar-s texture, with a light grey colour. Chert is white in colour. D2 is seen in the centre of the image, dark brown in colour; (F) CL of E, D1 presents bright orange-yellow luminescence. Chert is non-luminescent. D2 presents a dull red colour.
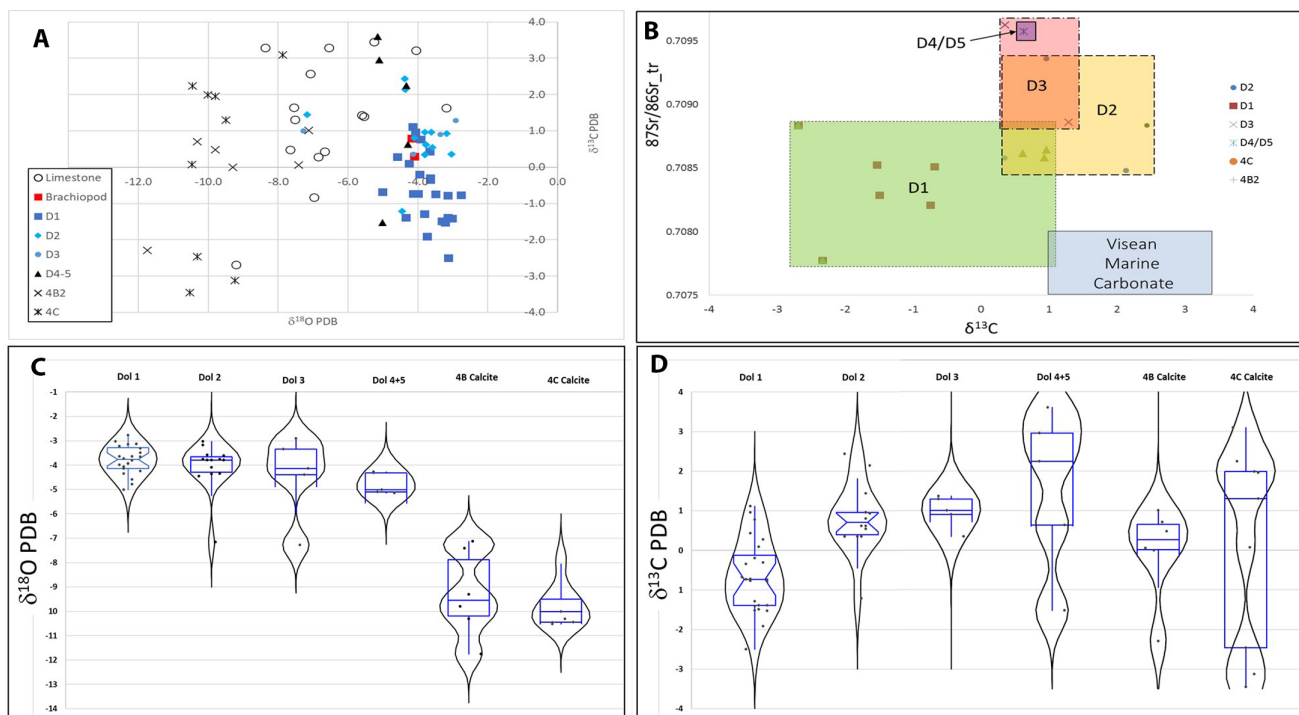
FIGURE 6 Isotope data for dolomite phases D2–D5; (A) $\delta^{13}C$ and $\delta^{18}O$ values for dolomite cement phases D2–D5, alongside D1 dolomite and calcite phases 4B and 4C (from Breislin et al., 2020), unaltered brachiopods and Visean limestone. Note the wide range of $\delta^{18}O_{limestone}$ values reflecting the widely varying abundance of pore filling Zone 3 and Zone 4 calcite (Walkden & Williams, 1991) which often have low $\delta^{18}O_{calcite}$ values; (B) strontium isotopic compositions D2–D5 dolomite, post dolomitisation calcite cements, 4B2 and 4C, along with Visean marine carbonate and dolomite phase D1 from Breislin et al. (2020). (C) Box and violin plots for $\delta^{18}O$ and (D) box and violin plots for $\delta^{13}C$ values using excel plug-provided by J. Dunham (GitHub—jdunham76/Mountjoy3: Microsoft Excel Templates for Statistical Graphs). The bottom line of the box is the 25th percentile; the horizontal line near the middle of the box is the median value (50th percentile), and the top of the box is the 75th percentile. The whiskers show the full data range. The 'violin' surrounding the box indicate the data density distribution, with the highest data density having the widest area and narrow areas indicating low data density or no data.

FIGURE 7 Rare earth element (REE) profiles of dolomite D2, D3 and post dolomitisation calcite cements 4B and 4C. Also presented is dolomite D1 and Visean marine carbonates as presented in Breislin et al. (2020).
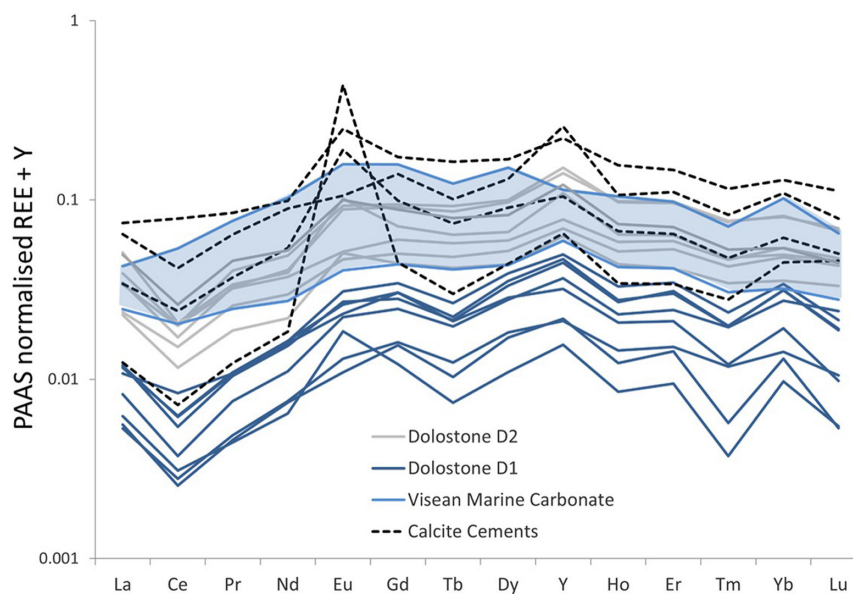
shows depletion in cerium and enrichment in yttrium. Fluid inclusion microthermometry was conducted on two samples of D2, with Th values ranging from 87 to 126°C

and salinities calculated from final ice melting (T_m) temperatures ranging from 7.3 to 13.4 wt% NaCl equivalent, with an average of 10.4 wt% NaCl equivalent (Figure 8).

6.3 | Dolomite D3

Dolomite phase 3 (D3) is non-fabric selective, non-stratabound and fabric destructive, occurring within Asbian and Brigantian platform interior and platform margin grainstone, packstones and mudstones (Figure 9). From field and core data, this phase of dolomitisation is estimated to form <10% of the total dolomite volume on the Derbyshire Platform. It occurs as dolomitised halos distinctly around N–S trending faults and fractures, ranging in thickness from 20 cm to 2 m. These faults and fractures cross-cut E–W orientated faults and dolomite

phases D1 and D2. D3 dolomite recrystallises the walls of fractures and replaces angular wall rock fragments within mosaic-breccias in calcite cemented fractures (Figure 10).

Typically, D3 dolomite is grey, fine-medium crystalline, and therefore similar in appearance to D2 dolomite, although zebra fabrics are occasionally developed. It is composed of dark brown, planar-s to non-planar inclusion rich rhombs (Figure 11). Crystal sizes range from 0.1 to 0.6 mm, and therefore smaller than D2 and being coarsest where D3 is replacing D2, usually most clearly visible near fractures. Phase D3 is best distinguished from phase
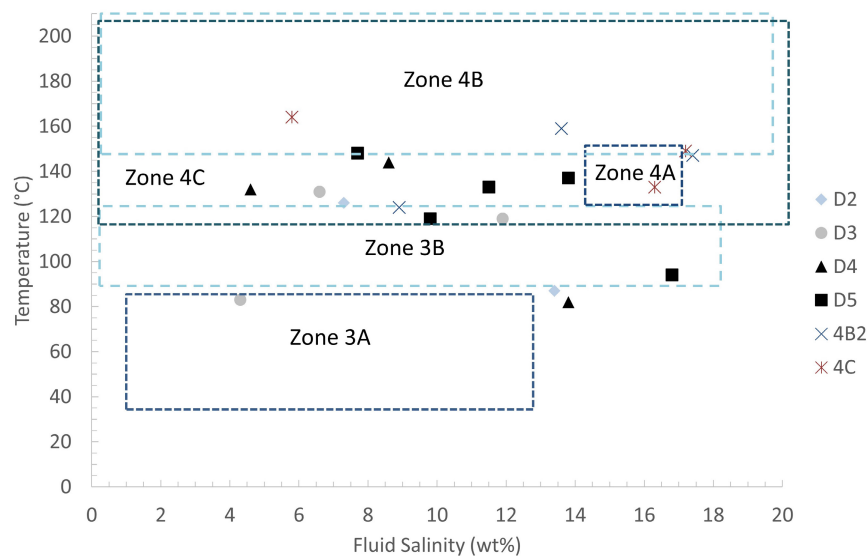

FIGURE 8   Fluid inclusion microthermometry data for dolomite phases D2, D3, D4 and D5, as well as calcite cement phases 4B and 4C in this study. Also included is calcite cement Zones 3A, 3B, 4A, 4B and 4C from Hollis (1998).
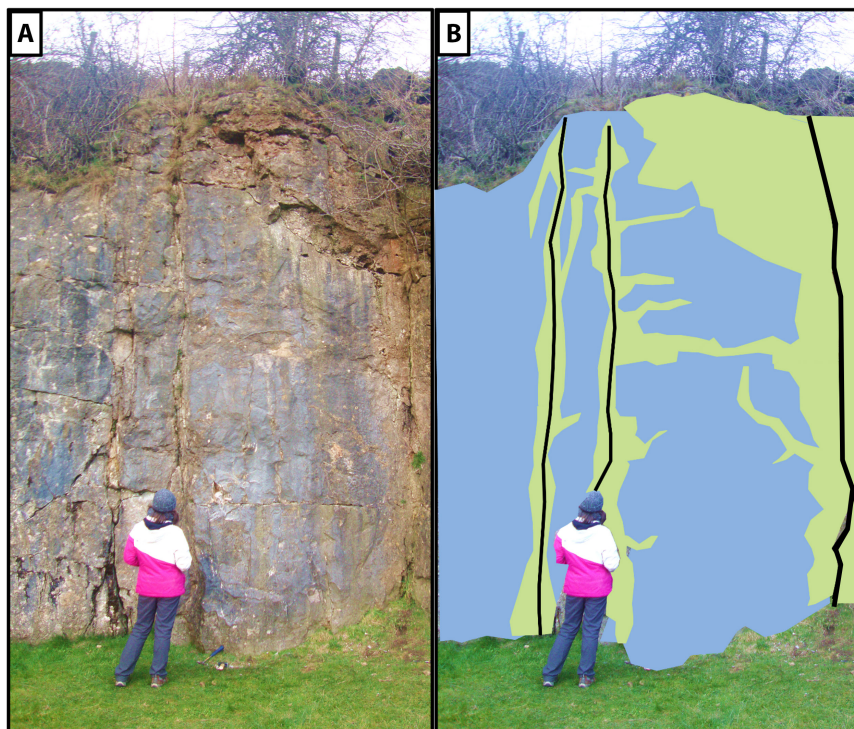

FIGURE 9   Brassington quarry. N–S orientated faults within massively bedded platform carbonates (blue). Faults display halos of dolomite D3 (green), with sharp terminations into the limestone.
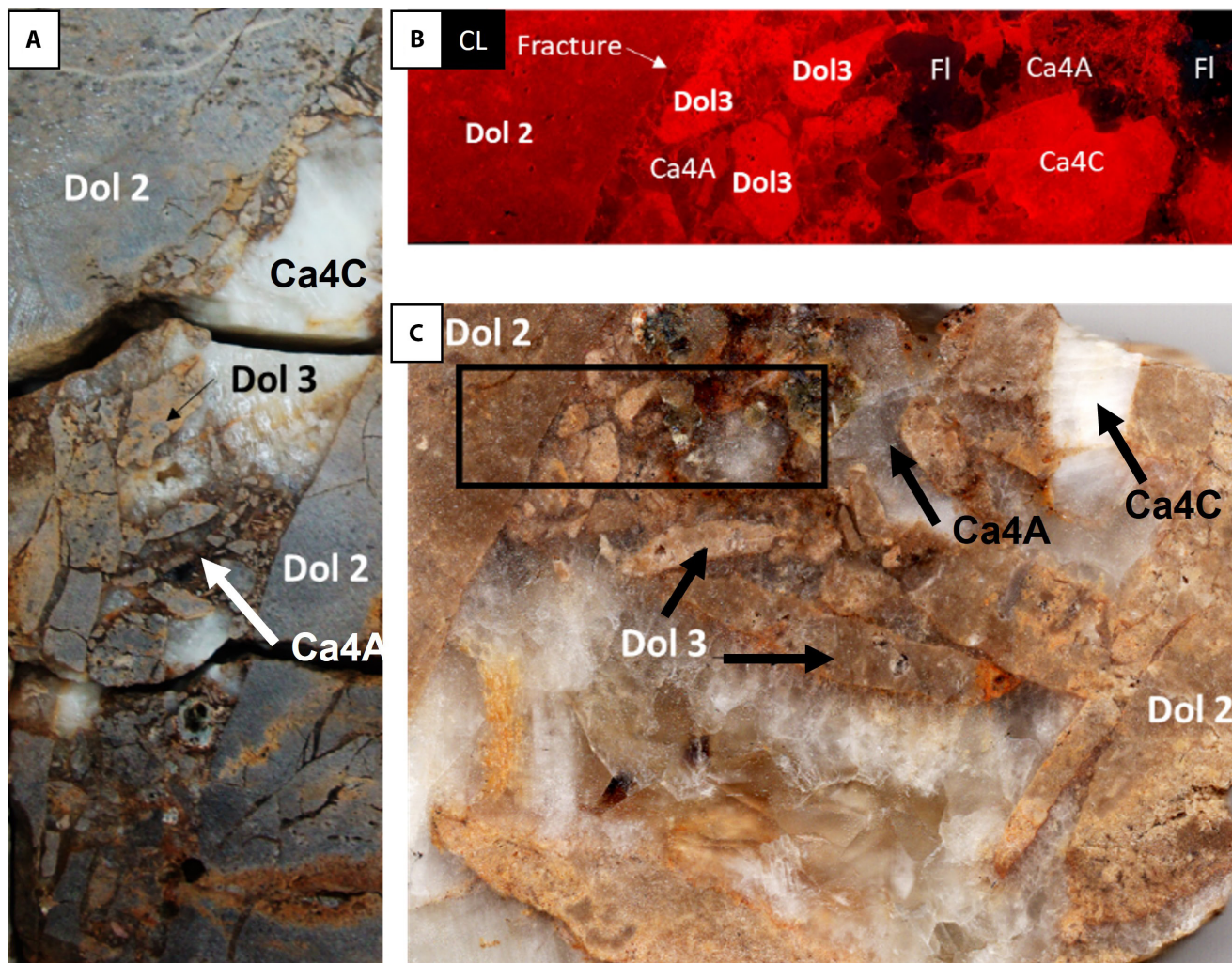
FIGURE 10 Association of dolostone phase D3 with faults and fractures; (A) Dolostone phase D3 within fracture cutting D2 dolomite. Fracture also infilled by calcite phase Ca4C (B) CL, D2 displays dull red luminescence, with D3 displaying bright red luminescence. Calcite cements within the fracture are Zone 4A with dull red luminescence, and Zone 4C with bright luminescence. Fluorite has dull blue luminescence; (C) Dolostone phase D3 associated with fracture. Fracture occurs within dolostone D2. Fracture wall rock and fragments within the fracture show recrystallisation by D3. Fracture is filled by later calcite cement. Box marks position of CL image in (B)

D2 under CL, where it is dull red, contrasting the bright red luminescence of D2 (Figure 10). Often D3 forms clear rims to turbid D2 crystals, and here the luminescence also changes form bright red D2 cores to dull red D3 rims. The overall effect of replacement of D2 by D3 is patchy mottled luminescence under CL (Figure 11).

The isotopic values of D3 range from $\delta^{13}C = 0.4$ to $1.4‰$ and $\delta^{18}O = -2.9$ to $-7.3‰$ (n.5) (Figure 6). The mean $\delta^{13}C$ values ($\delta^{13}C = 1‰$ n.5) of the dolomite are similar to slightly enriched in comparison to whole rock limestone and brachiopods ($\delta^{13}C$ values $= 1.2‰$ and $0.5‰$ respectively). The strontium ratio is $^{87}Sr/\,^{86}Sr = 0.7089$ (± 0.00004) (n.1) (Figure 6B). D3 dolomite contains two-phase fluid inclusions, including hydrocarbon inclusions. Fluid inclusion microthermometry was carried out on three samples. The Th values range from 83 to 131°C (n.3)

and salinities calculated from final ice melting (T_m) temperatures range from 6.6 to 11.9 wt% NaCl equivalent, with an average of 7.6 wt% NaCl equivalent (Figure 8).

6.4 | Dolomite D4

Dolomite phase D4 is volumetrically minor, forming <5% of the total dolomite volume. It occurs as a fracture lining and filling cement, as well as a very rare replacive phase that nucleates along fracture walls and stylolites, creating halos from <1 mm to 50 cm thick (Figure 12). The replacive dolomite is light grey and has a saddle dolomite texture (sensu Radke & Mathis, 1980), distinguishing it from D1 to D3 dolomite, and the thickness of the halo increases with the fracture width. D4 fracture cement is
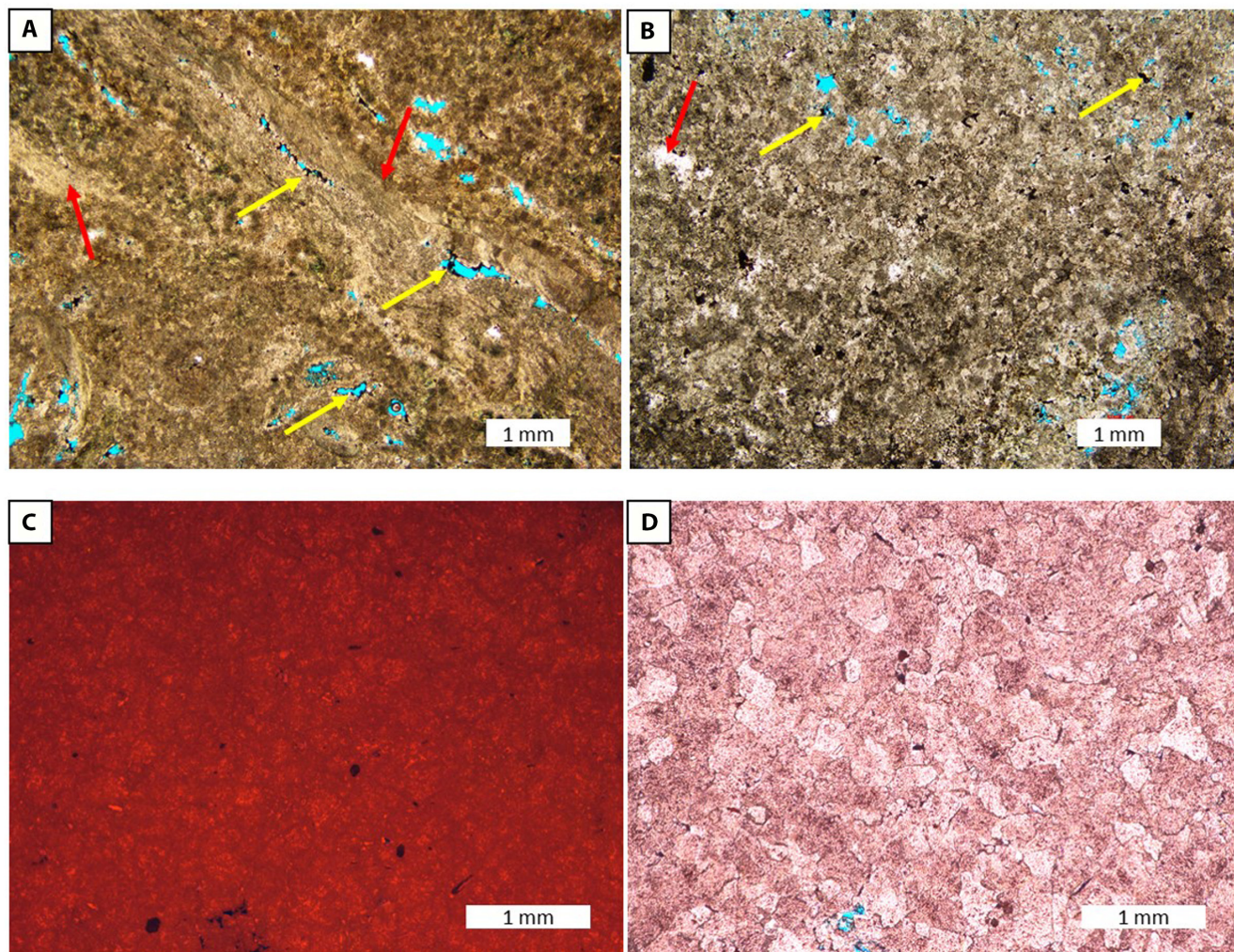
FIGURE 11 D3 petrography; (A) PL, planar-s – Non-planar D3. Turbid fluid inclusion density within cores. Ghost allochems of brachiopods remain (red arrows). Intercrystalline porosity developed, lined by bitumen (yellow arrows); (B) PL, non-planar, inclusion rich D3, with intercrystalline porosity lined by bitumen (yellow arrows) and post-dolomitisation calcite cement occluding porosity (red arrow); (C) CL, planar-s to non-planar D3 displaying mottled dull red luminescence (D) PL, planar-s to non-planar dolomite crystals have high inclusion density, and visible porosity is low.

composed of red-pink, turbid and limpid non-planar saddle dolomite crystals that range from <0.1 to 0.4 mm long. Under CL it has a dull red luminescence, but has a yellow luminescence where it is dedolomitised (Figure 13).

D4 is only found within 1 km of the platform margin along N–S and NW–SE orientated faults and fractures. These N–S faults show reactivation, after D3 dolomite, forming fracture-breccias with angular wall-rock fragments that show little rotation (Figure 12). A common feature of these fractures is that they are lined (where fractures are >3 mm wide) and bridged (where fractures are <3 mm wide) by pink-red D4 dolomite cements and occluded by calcite, fluorite, baryte and galena (Figure 12). D4 cross-cuts dolomite phases D1, D2 and D3, as well as forming within undolomitised limestone.

D4 and D5 dolomite cement could not be separated for stable isotopic analysis, and their undifferentiated

values are $\delta^{13}C = -1.5$ to 3.6‰ and $\delta^{18}O = -4.3$ to -5.2‰ (n.5) (Figure 6). The strontium ratio of dolomite D4/5 is $^{87}Sr/^{86}Sr = 0.7096$ (± 0.00004) (n.1) (Figure 6B,C) with a strontium concentration of 81.3 ppm (n.1). Fluid inclusion microthermometry was carried out on three samples of saddle dolomite cement phase D4. The Th values range from 82 to 144°C (n.3) and salinities calculated from final ice melting (T_m) temperatures to range from 4.6 to 13.8 wt% NaCl equivalent, with an average of 9 wt% NaCl equivalent (Figure 8).

6.5 | Dolomite D5

Dolomite phase D5 is volumetrically very minor, forming <5% of the total dolomite volume. It occurs as a fracture lining, bridging and filling cement. It usually occurs in fractures formed close to the platform margin along the same

FIGURE 12 Fracturing within N–S faults and host dolostone D3; (A) field photograph of N–S fault with large fracture containing angular clasts of wall rock D3 in the fracture, displaying little rotation. D4 is seen to form a bridging cement within these fractures. Black box marks position of (B); (B) rock slab from centre of fracture showing the angular clasts of D3 wall rock lined by dolomite cement D4. D4 is seen to form rims to these clasts as well as bridges between them. D5 then forms a lining cement to D4, and remaining fracture space is filled by Zone 4 calcite cements.
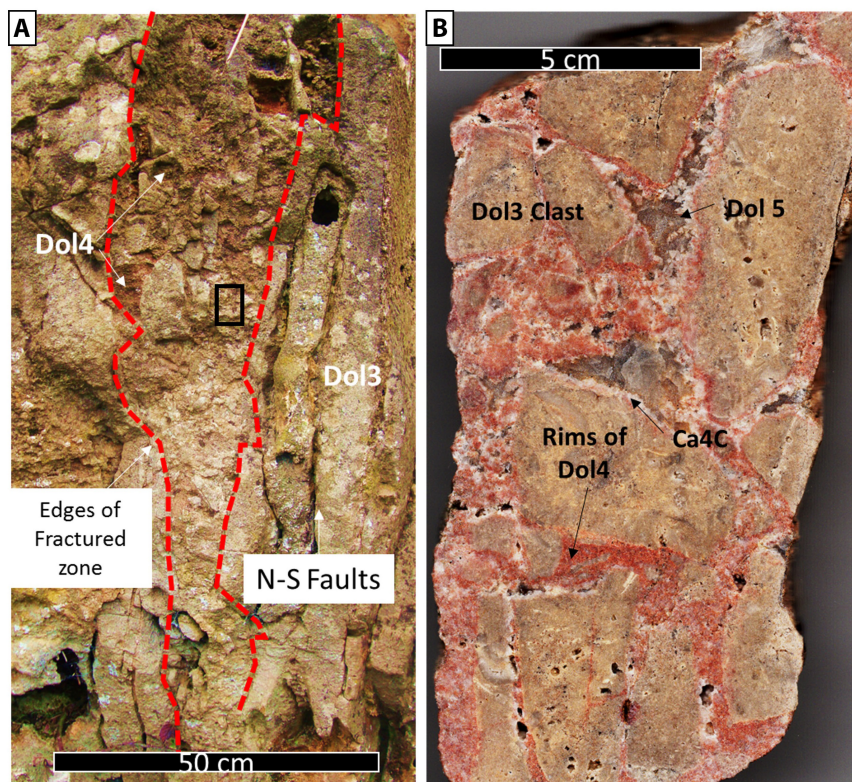
reactivated N–S and NW–SE orientated faults and fractures as D4 (Figure 12). It cross-cuts phases D1, D2, D3 and D4, as well as occurring within undolomitised limestone. Phase D5 is white in colour (Figures 12 and 13), contrasting the red-pink colour of D4. It fills fractures that are up to 3 mm wide and lines fractures that are up to 1 cm wide (Figures 12 and 13). Some of the wider fractures contain both D4 and D5 and rotated fragments of dolomitised wall rock and/or limestone, as well as some minor fluorite (Figure 14). In thin section, D5 is composed of white, cloudy, inclusion rich saddle dolomite crystals (Figures 13 and 14) that are 0.3–0.8 mm long and occasionally corroded. Under CL, D5 has a bright red luminescence, except where it is dedolomitised, when it becomes non-luminescent (Figure 14).

Fluid inclusion microthermometry was carried out on five samples of D5 dolomite cement, giving Th values from 94 to 148°C (n.5) and salinities calculated from final ice melting (T_m) temperatures that range from 9.8 to 16.8 wt% NaCl equivalent, with an average of 11.9 wt% NaCl equivalent (Figure 8).

6.6 | Post-dolomitisation fracture calcite cements

Calcite cements post-date dolomite phases D4 and D5, usually occluding fractures (Figures 10, 13 and 14). These calcite cements post-date dissolution of D4 and D5 dolomite, with the core of D5 crystals often being preferentially corroded (Figure 14). Two phases of cement are usually identified; the first phase is Zone 4B2, which is ferroan and dark brown to non-luminescent and usually occurs in minor volumes. The second phase, Zone 4C, is non-ferroan, blocky and forms most of the calcite cement. It has a bright yellow-orange luminescence and is often intergrown with fluorite, baryte and galena (Figures 13 and 14).

Calcite cement Zone 4B has isotopic values that range from $\delta^{13}C = 1$ to $-2.3‰$ and $\delta^{18}O = -7.1$ to -11.7 (n.6) (Figure 6). The $\delta^{13}C$ values of the calcite cement Zone 4C range from 3.1 to $-3.5‰$ and $\delta^{18}O = -7.9$ to -10.5 (n.9) (Figure 6). Calcite cements show enrichment in europium and yttrium relative to the dolomite, whole rock limestone and brachiopod samples (Figure 7). Phase Zone 4B calcite has Th values that range from 124 to 159°C (n.3) and salinities calculated from final ice melting (T_m) temperatures of 8.9 to 17.4 wt% NaCl equivalent, with an average of 13.3 wt% NaCl equivalent (Figure 8). Phase Zone 4C calcite cement has Th values that range from 133 to 164°C (n.3) and salinities calculated from final ice melting (T_m) temperatures that range from 5.8 to 17.2 wt% NaCl equivalent, with an average of 13.1 wt% NaCl equivalent (Figure 8).
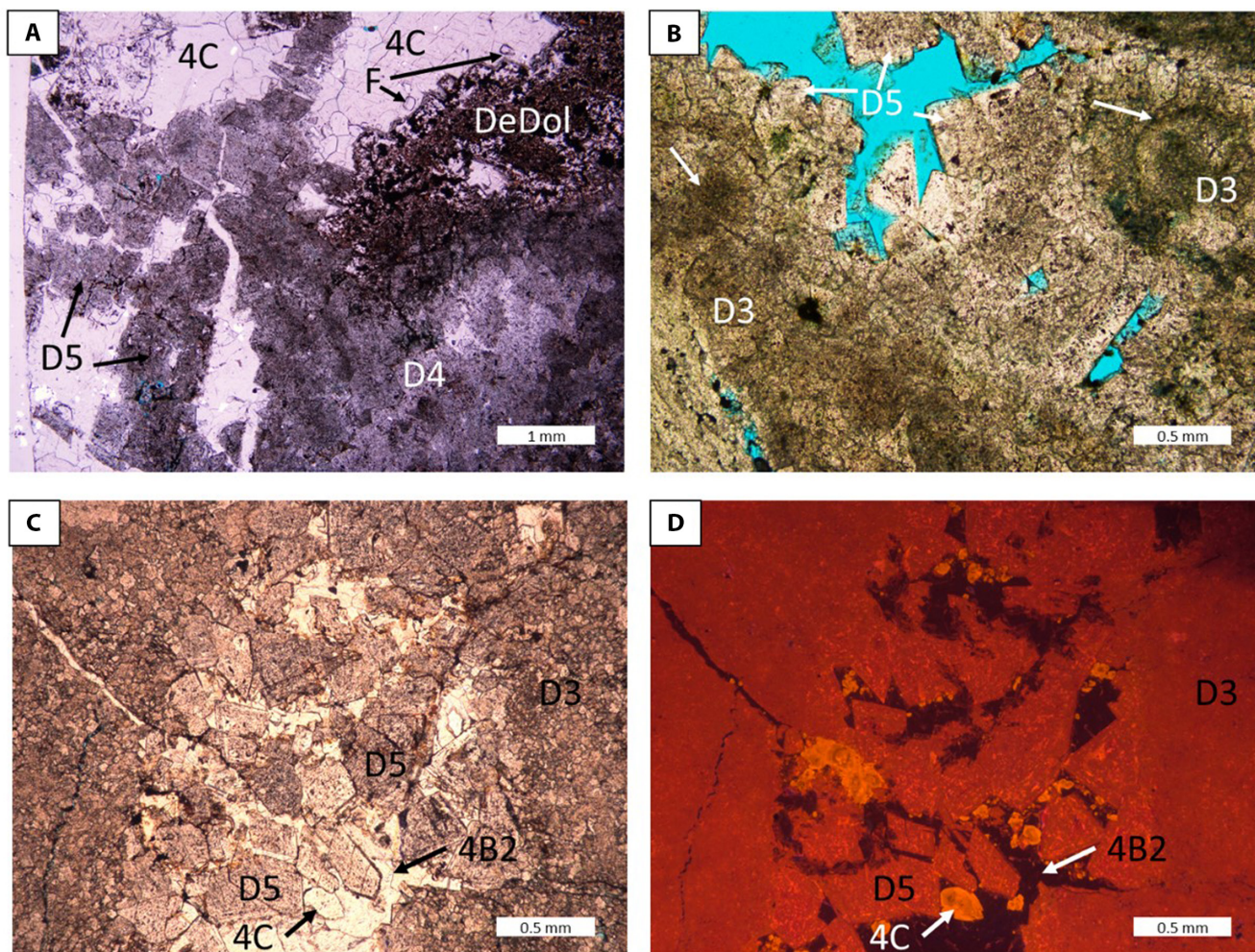
FIGURE 13 D4 and D5 petrography; (A) PL, fracture lining dolomite cements D4 and D5. D4 forms a non-planar mosaic, with D5 forming as isolated saddle crystals in the fracture. D4 and D5 show dedolomitisation (DeDol) with later calcite cement 4C filling remaining fracture space, as well as hosting fluorite mineralisation (F). (B) PL, D5 (arrowed) saddle dolomite crystals lining a fracture in D3. Ghost allochems observed within D3 fabric (arrowed). D5 show bitumen linings to crystals, and fracture space remains open; (C) PL, D5 saddle dolomite crystals line a fracture in D3. Post-dolomitisation calcite cements 4B2 and 4C (arrowed) fill remaining fracture space; (D) CL, D5 saddle dolomite crystals show mottled dull-bright red luminescence. D3 displays mottled dull red luminescence. Post-dolomitisation calcite cement 4B2 (arrowed) is non-luminescent and 4C (arrowed) displays bright yellow luminescence, with sector zoning.

7 | INTERPRETATION

7.1 | Distribution and relative timing of dolomitisation

Both D2 and D3 dolomite are fabric destructive non-planar, non-facies selective and non-stratabound, replacing limestone in proximity to faults and fractures, with their texture suggestive of precipitation above *ca* 50°C (Sibley & Gregg, 1987). They predominantly occur in the damage zones of major strike-slip faults and associated fractures, and in some places, they overprint precursor D1 dolomite. Phases D4 and D5 occur principally as cement fills of fractures, although phase D4 also locally replaces earlier phases. Phases D2–D5 dolomite all cross-cut

stylolites and therefore post-date pressure solution, implying formation at >300 m burial depth (Scholle & Ulmer-Scholle, 2003). All dolomite phases also post-date Zone 3 pore filling calcite cements which occlude much of the matrix porosity on the Derbyshire Platform, and which are interpreted to have formed during shallow burial and to be Serpukhovian in age (Hollis, 1998; Walkden & Williams, 1991).

D2 forms approximately 40% of the dolomite on the Derbyshire Platform. Each subsequent phase (D3–D5) decreases significantly in volume (Table 1) and becomes successively confined to fractures, with D4 and D5 forming as saddle dolomite cements. This suggests a decrease in permeability of the host rock and/or the supply of dolomitising fluids through time. D2 dolomite forms within
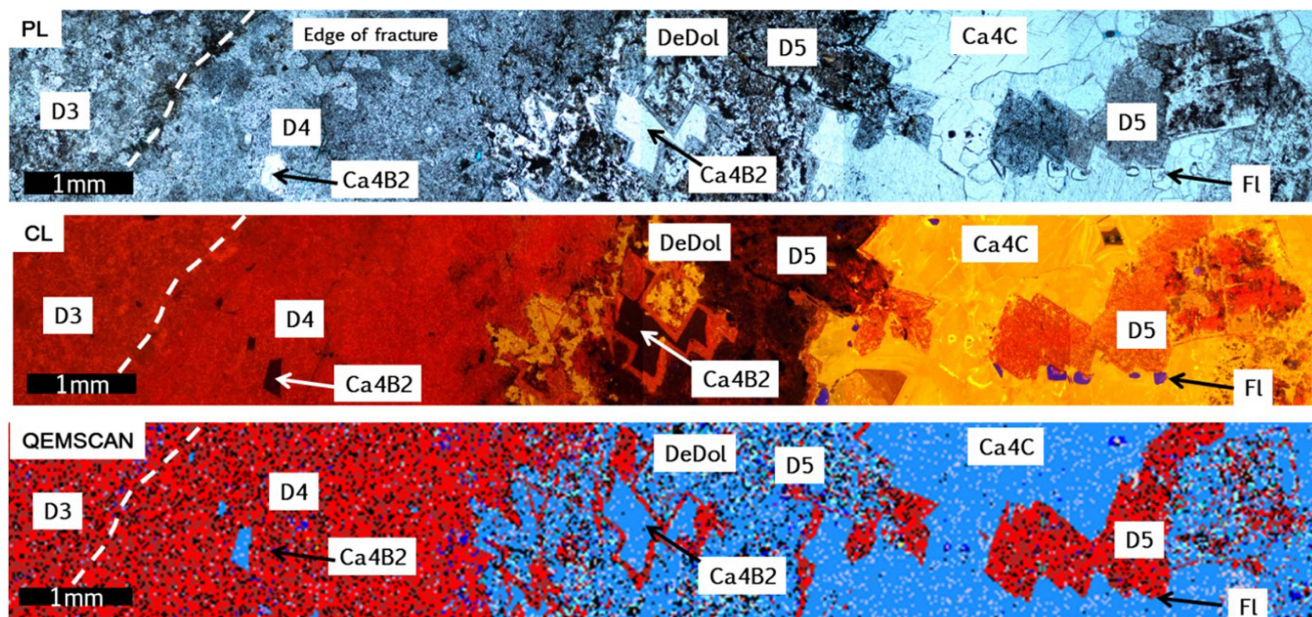
FIGURE 14 Post-dolomitisation calcite cement phases 4B2 and 4C within fracture hosted by dolomite phase D3. Fracture is lined by both D4 and D5 dolomite cements with calcite cements and mineralisation in the centre of the fracture; PL—Dolomite cements D4 and D5 lining the fracture display evidence of corrosion, with the centre of D5 crystals dissolved and filled with calcite cement (arrowed). Where dedolomitised, the dolomite crystals display a pitted appearance with an abundance of inclusions. Calcite cements filling pore space are blocky in texture, hosting minor fluorite (arrowed). CL—Where dedolomitisation is most intense, towards the centre of the fracture, dolomite luminescence changes from red to dark brown (DeDol). Two phases of calcite cement can be differentiated under CL. 4B2 is non-luminescent, and fills the centre of corroded dolomite crystals, as well as filling minor porosity within D4 (arrowed). D5 displays bright yellow luminescence. QEMSCAN) Dedolomitisation is highlighted under QEMSCAN, with the most intensely altered dolomite crystals mineralogy appearing as calcite (blue) rather than dolomite (red).

the damage zone of NW–SE orientated faults, particularly the crustal-scale Cronkston–Bonsall Fault, which suggests that these faults served as a conduit for high volumes of fluid that were driven along this basin-scale fault. In contrast, D3 dolomite forms halos around N–S orientated faults and fractures in significantly smaller volumes than D2. In places, angular wall rock fragments of D2 and D3 dolomite within these N–S faults are cemented by D4 and D5 dolomite. This implies multiple phases of fracturing and potentially high fluid pressures, while the occurrence of D4 as a bridging cement in some fractures implies syn-kinematic precipitation of dolomite within dilatational fractures (Phillips, 1972; Ukar & Laubach, 2016). Where fractures remained partially open, D5 dolomite, calcite, fluorite, baryte and galena were able to subsequently occlude fracture porosity, indicating that dolomitisation pre-dated mineralisation.

Both D4 and D5 dolomite cements often display corrosion and dedolomitisation where fractures are later filled by calcite cements (Zones 4B-C) that are intergrown with fluorite, baryte and galena (Figure 14). In particular, Zone 4B and 4C cements fill the centre of D5 dolomite crystals that were preferentially corroded, suggesting that dedolomitisation occurred immediately prior to or

during calcite cementation. The blocky texture of Zone 4C calcite that surrounds and post-dates D4 and D5 dolomite, with no evidence of fracturing of the bridging cement, suggests that it formed post-kinematically (Ukar & Laubach, 2016). Precipitation of Zone 4C calcite has previously been interpreted to be synchronous with the main phase of mineralisation on the Derbyshire Platform (Hollis & Walkden, 1996, 2002), which is interpreted to have occurred in the latest Carboniferous to early Permian (Coleman et al., 1989; Frazer et al., 2014; Hollis & Walkden, 2002, 2012; Ixer & Vaughan, 1993; Quirk, 1987). This brackets the timing for dolomitisation to during or after the Pennsylvanian but before the Permian.

7.2 | Fluid composition and temperature

Homogenisation data from fluid inclusion analysis indicate minimum temperatures of formation of 82 to 148°C for all dolomite phases. The maximum depth of burial of the Visean – Serpukhovian boundary on the Derbyshire Platform was *ca* 2–3 km (Frazer et al., 2014). Therefore, the maximum temperature of the uppermost Visean assuming a geothermal gradient of 25°C/km and a surface

temperature of 20°C would have been <100°C. However, given that the modern geothermal gradient is *ca* 27–32°C, and the low thermal conductivity of the Serpuhkhovian mudrocks overlying the platform, the temperature of the Visean limestone during dolomitisation could have been much higher. Assuming a geothermal gradient of 30°C/km to account for this, the uppermost Visean could have had a maximum temperature of greater than *ca* 110°C. Since the homogenisation temperatures provide a minimum estimate of temperature of precipitation, this suggests that dolomitisation, and dolomite and calcite cement precipitation, was from hydrothermal fluids (i.e. at least 5–10°C hotter than the host rock, sensu Machel & Lonnee, 2002).

The oxygen isotopic composition of the fluids that precipitated the replacive dolomite, and dolomite cement was calculated using Muller et al. (2019), and the range of $\delta^{18}O_{water}$ data is shown in Table 3. Using the combined minimum Th and lightest $\delta^{18}O_{carbonate}$ values and the maximum Th and highest $\delta^{18}O_{carbonate}$ values (to give combined low and combined high cases), $\delta^{18}O_{water}$ values are calculated to range from 2.0 to 12.4‰ SMOW for D2–D3 and 4.6–12.4‰ SMOW for D4-D5. The high values of $\delta^{18}O_{water}$, combined with the high salinities (up to 16.8 wt% NaCl) is indicative of formational brines. The strontium signature of unaltered brachiopod shells is equivalent to Visean sea-water ($^{87}Sr/^{86}Sr = 0.7078$ [±0.00004]) (Breislin et al., 2020; Burke et al., 1982). All dolomite samples from D2–D5 are more radiogenic than both Visean sea-water and D1 dolomite ($^{87}Sr/^{86}Sr = 0.7083$ [±0.00004]). The increase in strontium isotopic ratios from D2 to D5 ($^{87}Sr/^{86}Sr = 0.7087–0.7097$ [±0.00004]; Figure 6) strongly suggesting that the dolomitising fluids had some interaction with siliciclastic sediments.

The oxygen isotopic composition of the fluids that precipitated Zones 4B and 4C calcite was calculated using Wostbrock et al. (2020), and the combined minimum Th and lightest $\delta^{18}O_{carbonate}$ values and the maximum Th and highest $\delta^{18}O_{carbonate}$ values (to give combined low and combined high cases). The $\delta^{18}O_{water}$ is calculated to range from 3.8 to 11.3‰ SMOW for 4B calcite and 5.8–10.9‰ SMOW for Zone 4C calcite (Table 3). These estimated values, coupled with the high salinities (up to 23.1 wt% equiv. NaCl) is consistent with previous data (Hollis & Walkden, 2002) and precipitation from formational brines.

8 | DISCUSSION

8.1 | Fluid source

Stable isotope and fluid inclusion data show there to be little variation among the dolomite phases D2 and D3, while

TABLE 3 Range of possible $\delta^{18}O_{water}$ values for each diagenetic phase, calculated Muller et al. (2019) for dolomite and Wostbrock et al. (2020) for calcite, and using maximum and minimum homogenisation temperatures and maximum and minimum $\delta^{18}O_{carbonate}$ values.

	Min TH °C	Max TH °C	Min TH °K	Max TH °K	Min δ18Ocarb PDB	Max δ18Ocarb PDB	Min δ18Ocarb SMOW	Max δ18Ocarb SMOW	Min δ18Ocarb / Min TH δ18Owater SMOW	Max δ18Ocarb / Max TH δ18Owater SMOW	Max δ18Ocarb / Min TH δ18Owater SMOW	Min δ18Ocarb / Max TH δ18Owater SMOW
D2	87	126	360	399	−7.5	−3.0	23.2	27.8	2.9	11.8	7.5	7.2
D3	83	131	356	404	−7.9	−2.9	22.8	27.9	2.0	12.4	7.1	7.2
D4	82	144	355	417	−5.2	−4.3	25.5	26.5	4.6	12.1	5.5	11.1
D5	94	148	367	421	−5.2	−4.3	25.5	26.5	6.1	12.4	7.1	11.5
4B	124	159	397	432	−11.7	−7.1	18.8	23.6	3.8	11.3	8.5	6.6
4C	133	164	406	437	−10.5	−7.9	20.1	22.8	5.8	10.9	8.5	6.8

phases D4 and D5 appear shifted to lower $\delta^{18}O$ values (Figure 6), with all $\delta^{18}O_{dolomite}$ values higher than Zone 4B2 and Zone 4C calcite cements. All dolomite phases, except D1, have similar $\delta^{13}C$ values to Zone 4B2 and Zone 4C calcite cements (Figure 6). Fluid inclusion data show a range of temperatures and salinities, but typically D2–D5 were precipitated at over 100°C. This is significantly hotter than D1, which formed at <50°C (Breislin et al., 2020). The calculated range of $\delta^{18}O_{water}$ values is consistent with formational brines but is wide-ranging (Table 3). The significantly higher $^{87}Sr/^{86}Sr$ ratios for D2–D5, compared to D1, which formed from slightly modified sea-water (Breislin et al., 2020) suggests fluid interaction with clay minerals, which will have had a fundamental control on the Mg/Ca ratio of the fluid, as discussed below, as well as supplying base metals for mineralisation (Hollis & Walkden, 2002). Overall, the geochemical data are consistent with evolved basinal brines, therefore aligning with the conceptual model that dolomitising fluids were released along faults during compactional dewatering of overpressured Visean sediments within juxtaposed hangingwall basins (Frazer et al., 2014; Hollis & Walkden, 2012).

It is noteworthy that there is a wide range in temperature, $\delta^{18}O_{water}$ values and salinity for D2–D5 dolomite and Zone 4B-C calcite, suggesting that more than one fluid was present during dolomitisation and calcite cementation. This could be explained by the temporal evolution of fluids and/or the mixing of fluids from different compartments within the basins, particularly since the sedimentary succession in the basin contains variable volumes of carbonate, sandstone and mudstone as well as evaporites deep in the Widmerpool Basin (Hathern Anhydrite; Waters & Davies, 2006). In contrast, the $\delta^{13}C$ values of both replacive dolomite (D2–D3) and dolomite cement (D4–D5) is invariant and largely resembles the host limestone (Figure 6A). Similarly, REE profiles of both D2 and D3 have a similar profile to the brachiopod and whole rock limestones, implying rock buffering during dolomitisation, and therefore moderate to low fluid-rock ratios (Banner et al., 1988).

Visean sediments within the Edale, Widmerpool and Staffordshire basins contain limestone, dolomite, sandstone, mudrock and volcanic members (Fraser & Gawthorpe, 2003; Waters et al., 2009). Given the strong geochemical evidence for dolomitisation from basinal brines, the most likely source of magnesium for dolomitisation is clay diagenesis, particularly the transformation of smectite to mixed-layer illite–smectite and illite (Boles & Franks, 1979; MacHargue & Price, 1982). Fluid temperatures of 100–140°C are needed to release magnesium during this reaction (Elliot et al., 1999; Pollastro, 1993), and fluid inclusion microthermometry data from this study (83–148°C) are within that range. It is also possible that

the europium-anomaly seen in both phase D2 and calcite reflects alteration of feldspar and smectite to illite within the basins (Figure 7). However, it is highly likely that reactive magnesium-rich fluids would have precipitated magnesium-bearing minerals within the basin, reducing the potency of the dolomitising fluids. Analysis of the Visean and Serphukhovian succession in the Widmerpool Basin has indicated low volumes of magnesium-bearing clays, such as chlorite, but has shown that dolomite is common (Breislin, 2018; Hao et al., 2021).

Using geochemical models, Frazer (2014) and Frazer et al. (2014) accounted for intrabasinal consumption of magnesium and calculated that it was unlikely that sufficient ions could have been released to form all the dolomite observed on the Derbyshire Platform (which would require 1.82×10^{13} mol Mg). However, Frazer et al. (2014) noted that dolomitisation would have been possible if an earlier phase of dolomite ('seed dolomite') was present. Breislin et al. (2020) demonstrated that 50% of the volume of dolomite within the study area formed prior to burial, by geothermal convection of sea-water (D1), and therefore phases D2–D5 dolomite occupy an area of approximately 30 km^2. This would require approximately 0.9×10^{12} mol Mg which could more realistically be sourced from sediments in the surrounding basins. Supply of additional magnesium from other sources could also have increased the Mg/Ca ratio of the fluid. During formation of D1 dolomite, leaching of magnesium from olivine and pyroxene within intraformational mafic basalts, by reaction with fluids with a high pCO_2 has been invoked (Breislin et al., 2020; Frazer et al., 2014). Mafic basalts in both the Widmerpool Basin and on the Derbyshire Platform could have undergone continued alteration, supplying additional magnesium, during formation of D2–D5 dolomite, if CO_2 remained available to fluids from ongoing igneous intrusion. However, the age of the youngest igneous intrusions on the Derbyshire Platform is uncertain (Macdonald et al., 1986; Walters & Ineson, 1980). Since basinal extension had stopped and compressional tectonics initiated by the Moscovian (Fraser & Gawthorpe, 2003), it is possible that volcanism had waned and there was no longer a supply of reactive magmatic fluids that would have enhanced the potency of the dolomitising fluids.

8.2 | Timing of dolomitisation in the Pennine Basin

Dolomitisation of the Derbyshire Platform was a multiphase event, initiated by formation of D1 prior to burial to approximately 300 m burial and at temperatures of less than 50°C. This was coincident with rifting and the earliest phases of post-rift thermal subsidence in the late Visean to

Serphukhovian (Breislin et al., 2020). As cross-cutting relationships show that D2 formed after D1 (Figures 4 and 5), this provides the oldest possible age of formation for D2. Mineralisation post-dates dolomitisation and is fracture controlled, constraining the youngest possible age of dolomitisation on the Derbyshire Platform. Although the timing of mineralisation has never been conclusively established, there is strong field and petrographical evidence for calcite cementation, mineralisation and hydrocarbon emplacement during the Variscan Orogeny (Coleman et al., 1989; Dunham, 1983; Frazer et al., 2014; Hollis, 1998; Hollis & Walkden, 1996; Ixer & Vaughan, 1993; Quirk, 1987). In particular, a continuous sequence of calcite cementation on the Derbyshire Platform from successively hotter fluids, and with increasing intergrowth of fluorite, baryte and galena, suggests calcite cementation and mineral precipitation occurred either prior to or during basin inversion in the late Carboniferous to Permian. This interpretation is supported by preservation of Miocene Brassington Formation sediments, containing reworked Triassic sandstone, within fissures that cut both limestone and dolomite (Walsh et al., 2018) and which are thought to have initiated as hypogene caverns during mineralisation on the Derbyshire Platform (Ford, 2001; Walsh et al., 2018). Furthermore, within the diagenetic sequence, there is an absence of evidence for emergence and reburial, in contrast to the age—equivalent North Wales Platform (Juerges et al., 2016). In totality, this suggests that D2 dolomitisation occurred between the Serpukhovian and the Moscovian. Consistent with this interpretation, basin modelling suggests that overpressures within the basin would have been sufficiently high for rupture and expulsion of fluids from *ca* 306 Ma (Bashkerian) (Frazer et al., 2014).

8.3 | Relationship between dolomitisation, kinematic evolution and fluid flow

The kinematic evolution of the Derbyshire Platform is complex, and it is beyond the scope of this study to fully constrain it. However, there are clear relationships seen in the field between fault orientation and dolomite type which suggests a kinematic control on fluid flow and the distribution of dolomite, as summarised in Figure 15. The dominant NW—SE orientation of strike-slip faults on the platform is thought to reflect both the orientation of prior, Caledonian lineaments and the underlying basement, reactivated by regional extension in the Mississippian (Coward, 1993; Fraser & Gawthorpe, 2003; Leeder, 1988). The earliest phase of dolomitisation (D1) is commonly found along E–W trending faults, particularly in the southern part of the Derbyshire Platform, consistent with

N–S extension (Breislin et al., 2020). This suggests that although most movement during extension was along pre-existing structures, new faults were also formed, and that these faults were open to the sea floor, leading to seawater convection and dolomitisation in the latest Visean or earliest Serphukhovian (Breislin et al., 2020).

During the Serpukhovian to Bashkerian the Derbyshire Platform was undergoing thermal sag subsidence and the basin was filled by turbidite-fronted fluvio-deltaic sandstones and mudrocks (Frazer & Gawthorpe, 2003). D2 dolomite has been interpreted to be approximately Bashkerian in age, or younger, and its localisation along the Cronkston–Bonsall Fault therefore provides an indication of the timing of initiation of fault movement during basin inversion. Since the faults now have a strike-slip offset, fluid flow probably occurred by dilation along the fault plane. Initial rupture of overpressured compartments within the hangingwall basins, and seismic valving of fluids onto the Derbyshire Platform likely resulted in expulsion of large volumes of magnesium-rich fluid (Frazer et al., 2014). These fluids would have been rapidly transported onto the Derbyshire Platform, where they would have been in thermal and chemical disequilibrium with the host rock, leading to dolomitisation. The confinement of much of the D2 dolomite body to the damage zone of faults might reflect the low matrix porosity of the limestone. Cementation of matrix porosity had occurred prior to the formation of D1 (Hollis & Walkden, 2002; Walkden & Williams, 1991), and therefore fluid flow would have been facilitated by open faults and open fractures within the damage zone. Eventually dolomitisation occluded fracture porosity, confining fluid flow to the fault plane.

Dolomite phase D3 is found along N–S faults, while D4 and D5 cements are found within NW–SE and N–S orientated faults which are also commonly mineralised. The N–S faults often occur as splays to NW–SE trending faults and commonly display multiple fracture opening events, mosaic brecciation and zebra dolomite textures (Figures 10 and 12). This suggests high fluid pressures, with multiple phases of opening and cementation indicating episodic fluid flux. Field relationships are unclear, but these could be en echelon normal faults such as those that are commonly formed at releasing bends or horsetail splays (Christie-Blick & Biddle, 1985). The area of dolomitisation by D3 dolomite around N–S faults is minor (usually forming halos <10 cm wide). This lower volume of dolomite and restriction to narrower zones of replacement around fractures, compared to D2 (Figure 9), could reflect a decrease in the permeability of the host limestone, a decrease in the volume of water and/or lower potency of the dolomitising fluid. Furthermore, the progressive reduction in the volume of dolomite, and a change from replacive dolomitisation to dolomite cementation, suggests that fluid pressures were high.
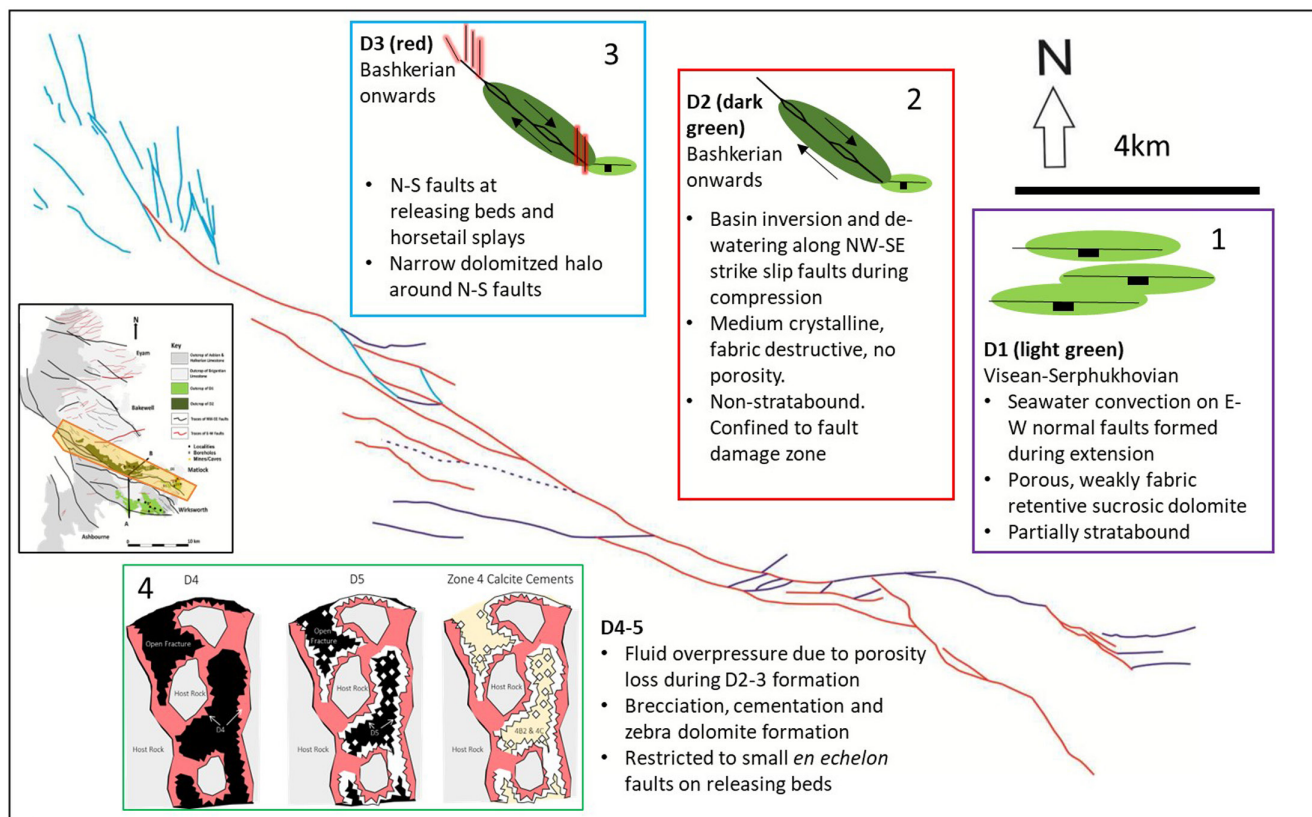
FIGURE 15 Summary of the relationship between the kinematic evolution of the Derbyshire Platform and dolomitisation based on the Cronkston–Bonsall Fault zone, highlighted in orange on the inset map (same as Figure 2) of the Derbyshire Platform. (1) North–south extension in the Visean led to sea-water convection along E–W trending faults (purple faults) forming D1 (light green bodies; see Breislin et al., 2020). (2) N–S directed compression from (approximately) the Bashkerian led to dewatering of hangingwall basins and formation of D2 within the damage zone of NW–SE oriented strike-slip faults (red faults surrounded by dark green bodies). These faults are reactivated, Caledonian-aged, crustal lineaments. (3) N–S trending faults within horse-tails along the Cronkston–Bonsall Fault (light blue faults) and en echelon faults formed at restraining bends (not shown) focus narrow halos of D3 dolomite (red bodies). (4) increasing fluid pressure along fault plane as porosity is occluded leads to brecciation along short N–S and NE–SW trending faults and cementation by D4 and D5 dolomite cements. Residual breccia porosity is occluded by Zone 4 calcite cements.

It has been shown that dolomitisation preceded mineralisation, and both D2–D5 dolomite and mineralisation are interpreted to have occurred by dewatering of basinal sediments during overpressure release. It is therefore reasonable to question whether dolomitisation from basinal brines depleted the volume of reactive fluids for subsequent mineralisation. However, basin models (Frazer et al., 2014) show that rupture of overpressured Visean sediments deep in the hangingwall basins, resulting in dolomitisation, could have facilitated the flux of mineralising fluids from Serpukhovian mudrocks that were juxtaposed and overlying the Derbyshire Platform. These mudrocks were potentially the principal source of lead and fluorine for galena and fluorite respectively, while barium could have been supplied from Serpukhovian-Bashkerian sandstones (Hollis & Walkden, 2002). Downward flux of these fluids could only have occurred if a pressure differential was set up by the dewatering of deeper sediments (Frazer et al., 2014). It is noteworthy that fault-controlled dolomitisation is restricted to

the southern part of the Derbyshire Platform, and the reasons for this are not clear. Hollis and Walkden (2002) noted the different composition of sediments in the Edale Basin compared to the Widmerpool Basin, with a high concentration of organic matter in the Edale Basin. It is possible, therefore, that fluids expelled from the Edale Basin had lower Mg/Ca ratios and therefore dolomitisation did not occur in the northern area.

9 | WIDER CONTEXT AND IMPLICATIONS

There has been much discussion in the last 20 years as to the source of fluids and magnesium for hydrothermal dolomitisation (HTD) (Bouch et al., 2004; Davies & Smith, 2006; Frazer et al., 2014; Gasparrini et al., 2006; Gregg, 2004; Hendry et al., 2015; Hollis et al., 2017; Iriarte et al., 2012; Juerges et al., 2016; Lapponi et al., 2014;

Lopez-Horgue et al., 2010; Machel, 1987; Mahboubi et al., 2016; Mountjoy et al., 1999; Swenen et al., 2003). It has become clear that there is unlikely to be a common model for all fault-controlled hydrothermal dolomite bodies, but that fault-plane convection of sea-water, fluid convection along basal aquifers and fluid mixing are all likely to be important controls on the localisation of dolomite bodies (Benjakul et al., 2020; Hollis et al., 2017; Koeshiydayatullah et al., 2020; Stacey et al., 2020, 2021). It has also become evident that in many bodies, progressive occlusion of porosity results in the back-stepping of reaction fronts in time so that fluid flux is constrained to fault planes, where fluid pressures can build (Koeshiydayatullah et al., 2021; McCormick et al., 2021; Stacey et al., 2021). This can lead to the formation of the most characteristic features of HTD; saddle dolomite cemented breccias and zebra dolomite textures.

In this study, fluid flux is interpreted to have occurred by dewatering of juxtaposed, hangingwall basins, but during the main phase of fault-controlled dolomitisation (D2), brecciation, saddle dolomite and zebra fabrics are not seen. It is not until later phases of dolomitisation, along N–S faults, that these more characteristic textures are observed and there is a change from replacement of wall rock to cementation of fractures. In this case, a back-stepping of the reaction front is less evident that in other studies (McCormick et al., 2021; Stacey et al., 2021), but instead high pressure fluids were focussed along narrow fault splays that appear to derive from the main NW–SE trending crustal lineament. However, the process is somewhat similar; fluid pressures built because matrix permeability had been reduced, forcing fluids to rupture the rock at high pressure, forming saddle dolomite cemented breccias and zebra textures. Since dolomitisation was taking place during the earliest phases of basin inversion, along a long-lived, crustal-scale strike-slip fault, it appears that the kinematics of this reactivation played a key role in directing fluid migration and reaction pathways. This further emphasises the importance of understanding the structural history of a basin when interpreting the genesis of fault-controlled dolomite bodies. It also strongly supports the notion that classic textures that are used to interpret fault-controlled, potentially hydrothermal, dolomite bodies in the field, such as brecciation and zebra dolomite formation, only form under particular conditions (Hollis et al., 2017), including under high fluid pressures created by injecting fluid into low permeability fracture zones.

10 | CONCLUSIONS

This study demonstrates the complex interplay between basin kinematics, host rock permeability and timing of fluid supply through episodic fault reactivation, connecting platforms to basin compartments, which ultimately controlled the positioning of fault-controlled dolomite on the Derbyshire Platform. The distribution, texture and geochemical fingerprint of the dolomites provide evidence for pulsed dewatering of basinal brines onto the Derbyshire Platform along pre-existing structural lineaments. The formation of dolomite during the earliest phases of fluid emplacement created a low permeability zone around faults, leading to an increasing confinement of dolomitisation to fractures. Eventually, high fluid pressures led to fluid release into N–S trending faults, which were subsequently brecciated and cemented. Fluid expulsion and dolomitisation took place in the Serpukhovian to Moscovian, most likely in the Bashkerian, when fluid pressures were high and Variscan tectonics had been initiated. Dolomitisation pre-dated mineralisation, which likely occurred as a result of fluid drawdown from overlying Serpukhovian to Bashkerian sediments during the latest Carboniferous and earliest Permian.

DATA AVAILABILITY STATEMENT
The geochemical data that support the findings of this study are available within the attached supplementary datafile. All other data are available on reasonable request to the authors.

ORCID
Cathy E. Hollis https://orcid.org/0000-0002-3980-2583

REFERENCES
Banner, J.L., Hanson, G.N. & Meyers, W.J. (1988) Rare earth element and Nd isotopic variations in regionally extensive dolomites from the Burlington-Keokuk formation (Mississippian):

implications for REE mobility during carbonate diagenesis. *Journal of Sedimentary Petrology*, *58*(3), 415–432.

Benjakul, R., Hollis, C., Robertson, H.A., Sonnenthal, E.L. & Whitaker, F.F. (2020) Understanding controls on hydrothermal dolomitisation: insights from 3D reactive transport modelling of geothermal convection. *Solid Earth*, *11*, 2439–2461. https://doi.org/10.5194/se-11-2439-2020

Boles, J.R. & Franks, S.G. (1979) Clay diagenesis in Wilcox sandstones of southwestern Texas: implications of smectite diagenesis on sandstone cementation. *Journal of Sedimentary Petrology*, *49*, 55–70.

Bouch, J.E., Milodowski, A.E. & Ambrose, K. (2004) Contrasting patterns of pore-system modification due to dolomitization and fracturing in Dinantian basin-margin carbonates from the UK. In: Braithwaite, C., Rizzi, G. & Darke, G. (Eds.) *The geometry and petrogenesis of dolomite hydrocarbon reservoirs*, Geological Society, London, Special Publications, London: Geological Society of London, *235*, pp. 325–348.

Breislin, C., Crowley, S., Banks, V.J., Marshall, J.D., Millar, I.L., Riding, J.B. & Hollis, C. (2020) Controls on dolomitization in extensional basins: an example from the Derbyshire platform, U.K. *Journal of Sedimentary Research*, *90*, 1156–1174. https://doi.org/10.2110/jsr.2020.58

Breislin, C.J. (2018). Basin-scale mineral and fluid processes at a platform margin, lower carboniferous, UK. PhD Thesis, University of Manchester, 236 pp.

Bridges, P.H. & Chapman, A.J. (1988) The anatomy of a deep water mud-mound complex to the southwest of the Dinantian platform in Derbyshire, UK. *Sedimentology*, *35*, 139–162.

Burke, W.H., Denison, R.E., Hetherington, E.A., Koepnick, R.B., Nelson, H.F. & Otto, J.B. (1982) Variation of seawater $^{87}Sr/^{86}Sr$ throughout Phanerozoic time. *Geology*, *10*, 516–519.

Charlier, B.L.A., Ginibre, C., Morgan, D., Nowell, G.M., Pearson, D.G., Davidson, J.P. & Ottley, C.J. (2006) Methods for the microsampling and high-precision analysis of strontium and rubidium isotopes at single crystal scale for petrological and geochronological applications. *Chemical Geology*, *232*, 114–133.

Christie-Blick, N. & Biddle, K. (1985) Deformation and basin formation along strike-slip faults. In: *Strike-slip deformation, basin formation and sedimentation*, SEPM Special Publication, Tulsa: Society for Sedimentary Geology, *37*, pp. 1–34.

Coleman, T.B. Jones, D.G, Plant, J.A. and Smith, K. (1989) Metallogenic models. In: J.A. Plant. and D.G. Jones (Eds.) *Metallogenic models and exploration criteria for buried carbonate-hosted ore deposits—a multidisciplinary study in eastern England: British Geological Survey, Keyworth, and institute of mining and metallurgy*. London: British Geological Survey and Institute of Mining and Metallurgy, pp. 123–134.

Collinson, J.D. (1988) Controls on Namurian sedimentation in the Central Province basins of northern England. In: Besly, B.M. & Keeling, G. (Eds.) *Sedimentation in a Synorogenic Basin complex. The upper carboniferous of Northwest Europe*. Glasgow: Blackie, pp. 85–101.

Corbella, M., Gomez-Rivas, E., Martín-Martín, J.D., Stafford, S.L., Teixell, A., Griera, A., Travé, A., Cardellach, E. & Salas, R. (2014) Insights to controls on dolomitization by means of reactive transport models applied to the Benicàssim case study (Maestrat Basin, eastern Spain). *Petroleum Geoscience*, *20*(1), 41–54. https://doi.org/10.1144/petgeo2012-095

Coward, M. (1993) The effect of late Caledonian and Variscan continental escape tectonics on basement structure, Palaeozoic basin kinematics and subsequent Mesozoic basin development in NW Europe. In: Parker, J.R. (Ed.) *Petroleum Geology of Northwest Europe: proceedings of the 4th conference*. London: Geological Society of London, pp. 1095–1108.

Davies, G. & Smith, L. (2006) Structurally controlled hydrothermal dolomite reservoir facies: an overview. *American Association of Petroleum Geologists Bulletin*, *90*, 1641–1690.

Deniel, C. & Pin, C. (2001) Single-stage method for the simultaneous isolation of lead and strontium from silicate samples for isotopic measurements. *Analytica Chimica Acta*, *426*(1), 95–103.

Dunham, K.C. (1983) Ore genesis in the English Pennines—a fluorite subtype. In: G. Kisvar-Sanyi, S.K. Grant, W.P. Pratt and J.W. Koenig (Eds.) *International conference on MVT lead-zinc deposits*. Proceedings volume, Rolla-Missouri: University of Missouri Press, pp. 86–112.

Ehrenberg, S.N., Eberli, G.P., Keramati, M. & Moallemi, S.A. (2006) Porosity-permeability relationships in interlayered limestone-dolostone reservoirs. *AAPG Bulletin*, *90*(1), 91–114. https://doi.org/10.1306/08100505087

Elliot, W., Edenfield, J., Wampler, M., Matisoff, G. & Long, P. (1999) The kinetics of the smectite to illite transformation in cretaceous bentonites, Cerro Negro, New Mexico, Clays and Clay Minerals, *47*, 286–296.

Ford, T. & Quirk, D. (1995) Mineralization of the south Pennines. *Geology Today*, *11*, 77–182.

Ford, T. D. (2001) The geology of the Matlock mines: a review. Mining History, The Bulletin of the Peak District Mines Historical Society, 14, No. 6, Winter.

Ford, T.D. (2002) Dolomitization of the carboniferous limestone of the Peak District: a review. *Amercian Geologist*, *15*, 163–170.

Fowles, J. (1987) Dolomitisation of the Derbyshire platform. Unpublished, University of Cambridge.

Fraser, A.J. and Gawthorpe, R.L. (2003) An atlas of Carboniferous Basin evolution in northern England memoirs of the Geological Society of London.

Frazer, M. (2014) Reconstruction of burial diagenetic processes in a post-rift regime. Unpublished PhD thesis, University of Manchester.

Frazer, M., Whitaker, F. & Hollis, C. (2014) Fluid expulsion from overpressured basins: implications for Pb-Zn mineralisation and dolomitisation of the East Midlands platform, northern England. *Marine and Petroleum Geology*, *55*, 68–86. https://doi.org/10.1016/j.marpetgeo.2014.01.004

Friedman, I. & O'Neil, J.R. (1977) Compilation of stable-isotope fractionation factors of geochemical interest. In: Fleischer, M. (Ed.) *Data of Geochemistry*, U.S. Geological Survey, Professional Paper 440-KK, 12. United States Geological Survey. https://pubs.er.usgs.gov/publication/pp440KK

Gasparrini, M., Bechstaedt, T. & Boni, M. (2006) Massive hydrothermal dolomites in the southwestern Cantabrian zone (Spain) and their relation to the late Variscan evolution. *Marine and Petroleum Geology*, *23*, 543–568.

Gawthorpe, R.L. (1987) Tectono-sedimentary evolution of the Bowland Basin, N England, during the Dinantian. *Journal of the Geological Society*, *144*, 59–71. https://doi.org/10.1144/gsjgs.144.1.0059

Goldstein, R. and Reynolds T.J. (1994) Systematics of fluid inclusions in diagenetic minerals: short course 31. SEPM, Society for Sedimentary Geology, 199 pp.

Gonfiantini, R. (1981) The δ-notation and the mass spectrometric measurement techniques. In: Gat, J.R. & Gonfiantini, R. (Eds.) *Stable isotope hydrology: deuterium and oxygen-18 in the water cycle*. Vienna: International Atomic Energy Agency, pp. 35–84.

Gregg, J.M. (2004) Basin fluid flow, base-metal Sulphide mineralization and the development of dolomite petroleum reservoir. In: Braithwaite, C., Rizzi, G. & Darke, G. (Eds.) *The geometry and Petrogenesis of dolomite hydrocarbon reservoirs. Geological society London Special Publications*, Glasgow: Blackie, *235*, pp. 157–175.

Guion, P.D. & Fielding, C.R. (1988) Westphalian a and B sedimentation. In: Besley, B.M. & Kelling, G. (Eds.) *Sedimentation in a synorogenic basin complex; upper carboniferous of NW Europe.* Glasgow: Blackie, pp. 153–177.

Gutteridge, P. (1987) Dinantian sedimentation and the basement structure of the Derbyshire dome. *Geological Journal*, *22*, 25–41.

Gutteridge, P. (1991) Aspects of Dinantian sedimentation in the Edale Basin, North Derbyshire. *Geological Journal*, *26*, 245–269.

Hao, J., Taylor, K. & Hollis, C. (2021) Mineral diagenesis and inferred fluids in basinal mudstones: the carboniferous Morridge formation, Widmerpool gulf, UK. *Marine and Petroleum Geology*, *134*, 105373. https://doi.org/10.1016/j.marpetgeo.2021.105373

Hendry, J.P., Gregg, J.M., Shelton, K.L., Somerville, I.D. & Crowley, S.F. (2015) Origin, characteristics and distribution of fault-related and fracture-related dolomitization: insights from Mississippian carbonates, Isle of Man. *Sedimentology*, *62*, 717–752. https://doi.org/10.1111/sed.12160

Hollis, C. (1998) Reconstructing fluid history: an integrated approach to timing fluid expulsion and migration on the carboniferous Derbyshire platform, England. In: Parnell, J. (Ed.) *Dating and duration of fluid flow and fluid-rock interaction*. Geological Society, London, Special Publications, London: Geological Society of London, *144*, pp. 153–159.

Hollis, C., Bastesen, E., Boyce, A., Corlett, H., Gawthorpe, R., Hirani, J., Rotevatn, A. & Whitaker, F. (2017) Fault-controlled dolomitization in a rift basin. *Geology*, *45*, 219–222. https://doi.org/10.1130/G38s394.1

Hollis, C and Walkden, G (1996) In: Strogen, P., Somerville, I. & Ll Jones, G. (Eds.) Use of burial diagenetic calcite cements to determine the controls upon hydrocarbon emplacement and mineralization on a carbonate platform, Derbyshire, England, recent advances in carboniferous geology. *Special Publication of the Geological Society of London*, *107*, 35–49.

Hollis, C. & Walkden, G. (2002) Reconstructing fluid expulsion and migration north of the Variscan Orogen, northern England. *Journal of Sedimentary Research*, *72*, 700–710.

Hollis, C. & Walkden, G. (2012) Burial diagenetic evolution of the lower carboniferous (Dinantian) of the southern margin of the Askrigg platform and a comparison with the Derbyshire platform. *Petroleum Geoscience*, *18*, 83–95. https://doi.org/10.1144/1354-079311-049

Ibrahem, Y., Morozov, V.P., El Kadi, M. & Alaa, A. (2021) Porosity enhancement potential through dolomitization of carbonate reservoirs, a case of study from the Euphrates Graben fields, East Syria. *Petroleum*. https://doi.org/10.1016/j.petlm.2021.05.005

Iriarte, E., Lopez-Horgue, M.A., Schroeder, S. and Caline, B., 2012. Interplay between fracturing and hydrothermal fluid flow in the Ason Valley hydrothermal dolomites (Basque-Cantabrian Basin, Spain). In: J. Garland, J.E. Nielson, S.E. Laubach and K.J. Whidden (Eds.) *Advances in carbonate exploration and reservoir analysis.* Geological Society of London Special Publications, London: Geological Society of London, *370*, 207–227.

Ixer, R.A. & Vaughan, D.J. (1993) Lead–zinc–fluorite–barite deposits of the Pennines, North Wales and the Mendips. In: Pattrick, R.A.D. & Polya, D.A. (Eds.) *Mineralization in the British Isles*. London: Chapman and Hall, pp. 55–411.

Juerges, A., Hollis, C., Marshall, J. & Crowley, S. (2016) The control of basin evolution on patterns of sedimentation and diagenesis: an example from the Mississippian great Orme, North Wales. *Journal of the Geological Society, London*, *173*, 438–456. https://doi.org/10.1144/jgs2014-149

Koeshidayatullah, A., Corlett, H. & Hollis, C. (2021) An overview of structurally-controlled dolostone – limestone transitions in the stratigraphic record. *Earth Science Reviews*, *220*, 103751. https://doi.org/10.1016/j.earscirev.2021.103751

Koeshidayatullah, A., Corlett, H., Stacey, J., Swart, P.K., Boyce, A., Robertson, H., Whitaker, F. & Hollis, C. (2020) Evaluating new fault-controlled hydrothermal dolomitization models: insights from the Cambrian dolomite, Western Canadian Sedimentary Basin. *Sedimentology*, *67*, 2945–2973. https://doi.org/10.1111/sed.12729

Korneva, I., Bastesen, E., Corlett, H., Eker, A., Hirani, J., Hollis, C., Gawthorpe, R.L., Rotevatn, A. & Taylor, R. (2018) The effects of dolomitization on petrophysical properties and fracture distribution within rift-related carbonates (Hammam Faraun fault block, Suez rift, Egypt). *Journal of Structural Geology*, *108*, 108–120. https://doi.org/10.1016/j.jsg.2017.06.005

Lapponi, F., Bechstadt, T., Boni, M. & Banks, D. (2014) Hydrothermal dolomitization in a complex geodynamic setting (Lower Palaeozoic, northern Spain). *Sedimentology*, *61*, 411–443.

Leeder, M.R. (1988) Recent developments in carboniferous geology: a critical review with implications for the British Isles and NW Europe. *Proceedings of the Geologists' Association*, *99*, 73–100.

Lopez-Horgue, M., Iriarte, E., Schroder, S., Fernandez-Mendiola, P.A., Caline, B., Corneyllie, H., Fremont, J., Sudrie, M. & Zerti, S. (2010) Structurally controlled hydrothermal dolomites in Albian carbonates of the Ason valley, Basque Cantabrian Basin, northern Spain. *Marine and Petroleum Geology*, *27*, 1069–1092.

Macdonald, R., Gass, K., Thorpe, I. & Gass, G. (1986) Geochemistry and petrogenesis of the Derbyshire carboniferous basalts. *Journal of the Geological Society of London*, *141*, 147–159.

MacHargue, T.R. & Price, R.C. (1982) Dolomite from clays in argillaceous marin associated carbonates. *Journal of Sedimentary Petrology*, *52*, 873–886.

Machel, H.G. (1987) Saddle dolomite as a by-product of chemical compaction and thermochemical sulfate reduction. *Geology*, *15b*, 936–940.

Machel, H.G. & Lonnee, J. (2002) Hydrothermal dolomite – a product of poor definition and imagination. *Sedimentary Geology*, *152*, 163–171.

Mahboubi, A., Nowrouzi, A., Al-Aasm, I., Moussavi-Harami, S. & Mahmudy-Gharaei, M.H. (2016) Dolomitization of the Silurian Niur formation, Tabas block, east Central Iran: fluid flow and dolomite evolution. *Marine and Petroleum Geology*, *77*, 791–805.

Manifold, L., Del Strother, P., Gold, D.P., Burgess, P. & Hollis, C. (2021) Unravelling evidence for global climate change in Mississippian carbonate strata from the Derbyshire and North Wales platforms, UK. *Journal of the Geological Society*, *178*, 2020–2106. https://doi.org/10.1144/jgs2020-106

Manifold, L., Hollis, C. & Burgess, P. (2020) The anatomy of a Mississippian (Visean) carbonate platform interior, UK: Depositional cycles, glacioeustasy and facies mosaics. *Sedimentary Geology*, *401*, https://doi.org/10.1016/j.sedgeo.2020.105633

McCormick, C., Corlett, H., Stacey, J., Hollis, C., Feng, J., Rivard, B. & Omma, J. (2021) Shortwave infrared hyperspectral imaging as a novel method to elucidate multi-phase dolomitization, recrystallization, and cementation in carbonate sedimentary rocks. *Scientific Reports*, *11*, 21732. https://doi.org/10.1038/s41598-021-01118-4

McCrea, J.M. (1950) On the isotope chemistry of carbonate and a palaeotemperature scale. *Journal of Physical Chemistry*, *18*, 726.

Mountjoy, E.W., Machel, H.G., Green, D., Duggan, J. & Williams-Jones, A.E. (1999) Devonian matrix dolomites and deep burial carbonate cements: a comparison between the Rimbey-Meadowbrook reef trend and the deep basin of west-Central Alberta. *Bulletin of Canadian Petroleum Geology*, *47*(4), 487–509.

Muller, I., Rodriguez-Blanco, J., Storck, J.-C, Santilli do Nascimento, G., Bontognali, T., Vasconcelos, C., Benning, L. & Bernasconi, S. (2019) Calibration of the oxygen and clumped isotope thermometers for (proto-) dolomite based on synthetic and natural carbonates. *Chemical Geology*, *525*, 1–17. https://doi.org/10.1016/j.chemgeo.2019.07.014F

Nance, W.B. & Taylor, S.R. (1976) Rare earth element patterns and crustal evolution-l. Australian post-Archean sedimentary rocks. *Geochimica et Cosmochimica Acta*, *40*, 1539–1551.

Omidpour, A., Mahboubi, A., Moussavi-Harami, R. & Rahimpour-Bonab, H. (2022) Effects of dolomitization on porosity – permeability distribution in depositional sequences and its effects on reservoir quality, a case study from Asmari Formation, SW Iran. *Journal of Petroleum Science and Engineering*, *208*, Part A, 109348. https://doi.org/10.1016/j.petrol.2021.109348

Phillips, W.J. (1972) Hydraulic fracturing and mineralization. *Journal of the Geological Society, London*, *128*, 337–359.

Pollastro, R.M. (1993) Considerations and applications on the illite-smectite goethermometer in hydrocarbon bearing rocks from Miocene to Mississippian age. *Clays and Clay Minerals*, *41*, 119–133.

Pollington, A.D. & Baxter, E.F. (2010) High resolution Sm–Nd garnet geochronology reveals the uneven pace of tectono-metamorphic processes. *Earth and Planetary Science Letters*, *293*(1–2), 63–71.

Quirk, D, 1987, Structure and genesis of the south Pennine Orefield. PhD thesis, University of Leicester.

Radke, B.M. & Mathis, R.L. (1980) On the formation and occurrence of saddle dolomite. *Journal of Sedimentary Research*, *50*, 1149–1168.

Rosenbaum, J. & Sheppard, S.M.F. (1986) An isotopic study of siderites, dolomites and ankerites at high temperatures. *Geochimica et Cosmochimica Acta*, *50*, 1147–1150.

Saller, A.H. & Dickson, J.A.D. (2011) Partial dolomitization of a Pennsylvanian limestone buildup by hydrothermal fluids and its effect on reservoir quality and performance. *AAPG Bulletin*, *95*, 1745–1762.

Schofield, K. & Adams, A. (1986) Burial Dolomitization of the woo dale Limestones formation (lower Carboniferous), Derbyshire, England. *Sedimentology*, *33*, 207–219.

Scholle, P. & Ulmer-Scholle, U. (2003) A color guide to the petrography of carbonate rocks: grains, textures, porosity, diagenesis. *American Association of Petroleum Geologists Memoir*, *77*, 473. https://doi.org/10.1306/M77973

Schultz, L.G. (1964) Quantitative interpretation of mineralogical composition from X-ray and chemical data for the Pierre shale. United States Geological Survey, Professional Paper, 391-C, 1–31.

Sibley, D. & Gregg, J. (1987) Classification of dolomite rock textures. *Journal of Sedimentary Research*, *57*, 967–975. https://doi.org/10.1306/212F8CBA-2B24-11D7-8648000102C1865D

Stacey, J., Corlett, H., Holland, G., Koeshidayatullah, A., Cao, C., Swart, P., Crowley, S. & Hollis, C. (2021) Regional fault-controlled shallow dolomitization of the middle Cambrian Cathedral Formation by hydrothermal fluids fluxed through a basal clastic aquifer. *Geological Society of America Bulletin*, *133*, 2355–2377. https://doi.org/10.1130/B35927

Stacey, J., Hollis, C., Corlett, H. & Koeshidayatullah, A. (2020) Burial dolomitization driven by modified seawater and basal aquifer-sourced brines: insights from the Middle and Upper Devonian of the Western Canadian Sedimentary Basin. *Basin Research*, *33*, 648–680. https://doi.org/10.1111/bre.12489

Swennen, R., Vandeginste, V. & Ellem, R. (2003) Genesis of zebra dolomites (Cathedral Formation: Canadian Cordillera fold and Thrust Belt, British Columbia). *Journal of Geochemical Exploration*, *78-79*, 571–577.

Ukar, E. & Laubach, E. (2016) Syn- and postkinematic cement textures in fractured carbonate rocks: insights from advanced cathodoluminescence imaging. *Tectonophysics Part A*, *690*, 190–205.

Vanstone, S. (1998) Late Dinantian paleokarst of England and Wales: implications for exposure surface development. *Sedimentology*, *45*, 19–37.

Walkden, G.M. (1972) The mineralogy and origin of interbedded clay wayboards in the lower carboniferous of the Derbyshire dome. *Geological Journal*, *8*, 143–159.

Walkden, G.M. & Williams, D.O. (1991) The diagenesis of the late Dinantian Derbyshire East Midland carbonate shelf, Central England. *Sedimentology*, *38*, 643–670.

Walsh, P., Banks, V., Jones, P., Pound, M. & Riding, J. (2018) A reassessment of the Brassington formation (Miocene) of Derbyshire, UK and a review of related hypogene karst suffosion processes. *Journal of the Geological Society*, *175*, J17–J29. https://doi.org/10.1144/jgs2017-029

Walters, S.G. & Ineson, P.E. (1980) Mineralisation within the igneous rocks of the south Pennine orefiled. *Bulletin of the Peak District Mines Historical Society*, *7*, 315–325.

Waters, C.N. & Davies, S.N. (2006) Carboniferous: extensional basins, advancing deltas and coal swamps. In: Brenchley, P.J. & Rawson, P.F. (Eds.) *The geology of England and Wales*. London: Geological Society of London, p. 559.

Waters, C.N., Waters, R.A., Barclay, W.J. & Davies, J.R. (2009) Lithostratigraphical framework for carboniferous successions of Southern Great Britiain (Onshore). *British Geological Survey Research Report*, *RR/09/01*, 184.

Whitaker, F., Smart, P. & Jones, G.D. (2004) Dolomitization: from conceptual to numerical models. In: Braithwaite, C., Rizzi, G. & Darke, G. (Eds.) *The geometry and Petrogenesis of dolomite hydrocarbon reservoirs*, *Geological Society, London, Special Publications*, London: Geological Society of London, *235*, pp. 99–139.

Wostbrock, J., Cano, E. & Sharp, Z. (2020) An internally consistent triple oxygen isotope calibration of standards for silicates,

carbonates and air relative to VSMOW2 and SLAP2. *Chemical Geology*, *533*, 119432. https://doi.org/10.1016/j.chemgeo.2019.119432

SUPPORTING INFORMATION

Additional supporting information can be found online in the Supporting Information section at the end of this article.

How to cite this article: Breislin, C. J., Banks, V. J., Crowley, S. F., Marshall, J. D., Millar, I., Riding, J. B. & Hollis, C. E. (2023). Mechanisms controlling the localisation of fault-controlled hydrothermal dolomitisation, Derbyshire Platform, UK. *The Depositional Record*, *9*, 734–758. https://doi.org/10.1002/dep2.214